AD-A033 699 CALIFORNIA UNIV BERKELEY DEPT OF MECHANICAL ENGINEERING F/G 20/4
NUMERICAL SOLUTION OF WATER WAVES PRODUCED BY EXPLOSIONS,(U)
SEP 74 S M ROSEN N00014-69-A-0200-1067
UNCLASSIFIED FM-74-11 NL

1 OF 1
AD A033699

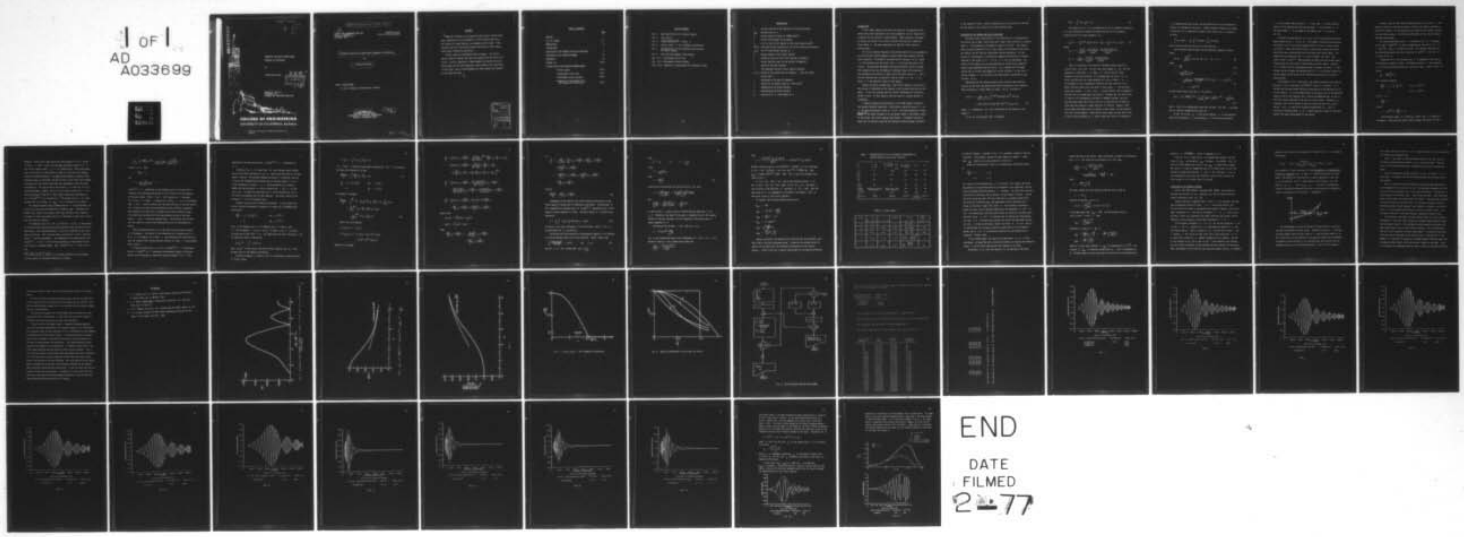

END

DATE FILMED
2-77

NUMERICAL SOLUTION TO WATER WAVES PRODUCED BY EXPLOSIONS

BY

Stanley Marc Rosen

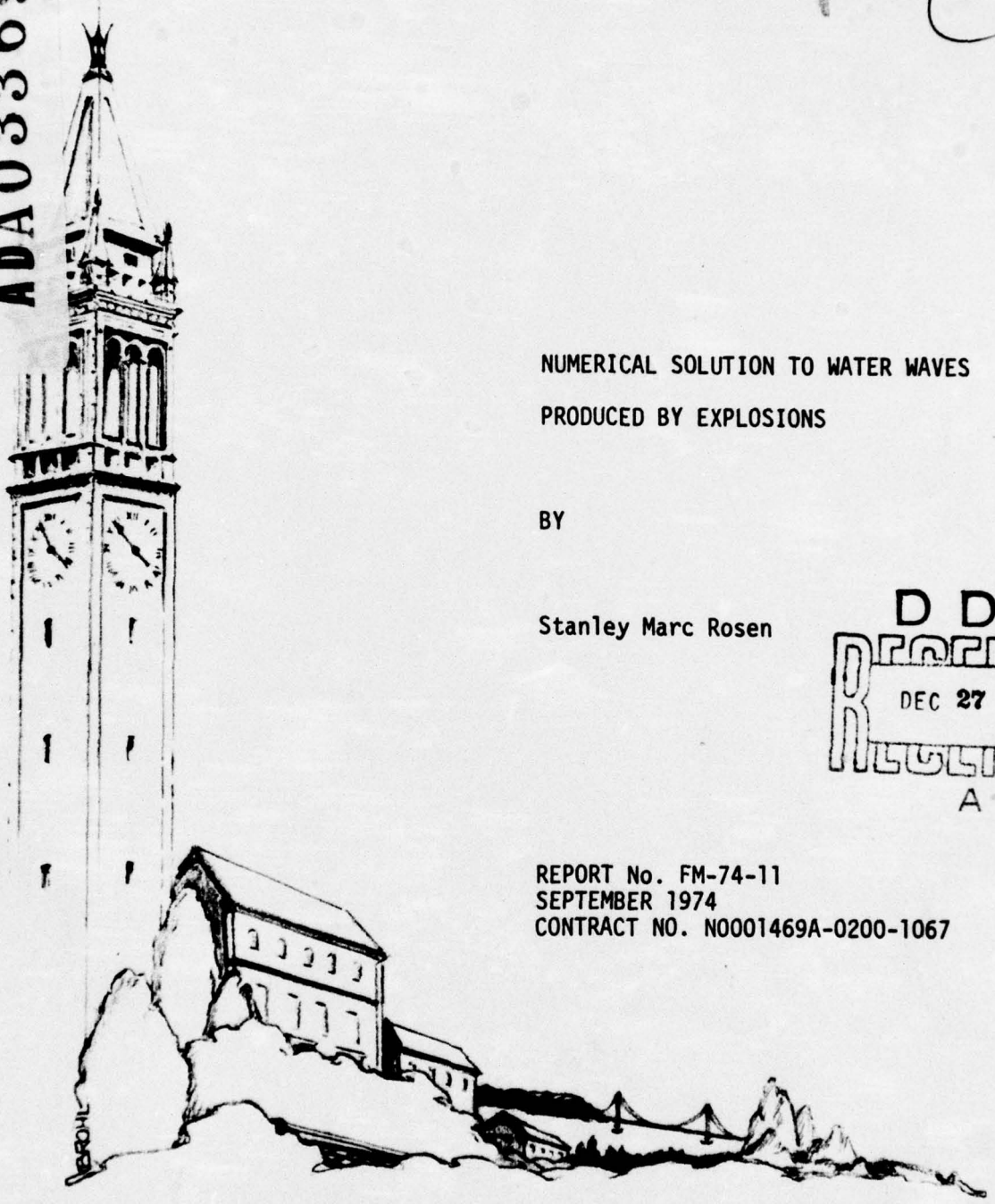

REPORT No. FM-74-11
SEPTEMBER 1974
CONTRACT NO. N0001469A-0200-1067

COLLEGE OF ENGINEERING
UNIVERSITY OF CALIFORNIA, Berkeley

(15) N00014-69-A-0200-1067

(14)

CONTRACT NO. N0001469A-0200-1067
REPORT NO. FM-74-11
SEPTEMBER 1974

SUPPORTED BY THE
OFFICE OF NAVAL RESEARCH

(6) NUMERICAL SOLUTION TO WATER WAVES PRODUCED BY EXPLOSIONS

BY

(10) Stanley Marc Rosen

FACULTY INVESTIGATOR:

M. Holt, Professor of Aeronautical Sciences

(11) SEPTEMBER 1974
(12) 49 p.

UNIVERSITY OF CALIFORNIA
DEPARTMENT OF MECHANICAL ENGINEERING
BERKELEY, CALIFORNIA 94720

400 426 bpg

ABSTRACT

Numerical solutions to the equations which govern surface water waves, generated by axially-symmetric initial impulses applied to the surface of a water medium, are presented in this paper. These equations were first derived by Kranzer and Keller in their paper, "Water Waves Produced by Explosions."

Several cases are considered within the paper. The initial impulse, depth of medium, and time and distance from the impulse are varied. Finally, comparison is made between the theoretically predicted waves and the waves measured at two different test conditions. In both cases, fairly close agreement was found between the theoretical and empirical data.

TABLE OF CONTENTS

LIST OF FIGURES

Nomenclature

A	variable portion of the amplitude of the wave envelope
A_{max}	maximum value of A
g	gravity constant (taken as .00980 Km/sec^2)
h	uniform finite depth of the medium
I_o	value of the initial impulse at the origin (dyne sec/cm^2)
$\bar{I}(\sigma/h)$	zero order Hankel transform of the initial impulse distribution
$J_x(y)$	the x^{th} order Bessel function of y
Q	energy content of the initial impulse
R	effective radius of the initial impulse (kilometers)
r	radius from the origin of the impulse (kilometers)
T	period of the wave (seconds)
t	time measured from the initial impulse (seconds)
$\eta(r,t)$	height of the surface wave at distance r from the origin, and at time t
λ	wavelength of the wave (kilometers)
ρ	density of the medium (taken as 1.025 Gr/cm^3)
σ	dimensionless auxiliary variable
ϕ	dimensionless auxiliary variable
ϕ'	derivative of ϕ with respect to σ

INTRODUCTION

In this paper numerical solutions are given for the equations which govern water waves generated by an axially-symmetric initial impulse which is applied on the surface of a water medium. These equations, developed by Kranzer and Keller,[1] are valid in the far field and for a medium of finite depth h. The waves generated will obey the linear theory of surface waves.

The initial impulse imparted to the uniform medium is axially-symmetric, and the resulting axially-symmetric surface water waves emanate from the source radially. The height of the water wave is denoted $\eta(r,t)$, where r is the distance from the origin, and t is the time from the initial impulse. The equations developed by Kranzer and Keller involve an asymptotic expansion and use the Method of Stationary Phase (first applied to this problem by Lord Kelvin in 1887), valid for large values of r and t, and can therefore only be applied in the far field, i.e., for $r >> R$, where R is the effective radius of the impulse.

Kranzer and Keller assumed that, "the initial impulse at any point in the surface is determined by the impulse in the incident shock wave at the point." It was also assumed that the initial displacement of the entire medium is zero. In this analysis only the case of a surface impulse is considered.

A computer program was developed for a CDC 7600 computer located at the Lawrence Berkeley Laboratory. With either a specified value of r or t, the program generates values of $\eta(r,t)$. The input parameters include density of the medium (assumed to be sea water), depth of the medium, radius of the charge, and initial impulse distribution. A graphical display of these data is possible using the GDS (Graphical Display System) available

in the computer library. Several postprocessors are available for the GDS, and the graphs in this report are of the microfiche type.

DISCUSSION OF THE KRANZER AND KELLER EQUATIONS

The medium under consideration is one consisting of an incompressible fluid which has an upper free surface and a lower rigid surface at a constant depth h. The boundary of the medium is taken at infinity. This implies that any waves produced will be a direct effect of disturbances from within the medium, and not from any reflections from the boundaries. For the source of a disturbance, a cylindrically symmetric distribution of impulse imparted at the origin (i.e., $r = 0$) at $t = 0$ will be considered. The result of this impulse will be the generation of cylindrically symmetric surface waves emanating from the origin. It is assumed that the upper surface has no initial displacement nor initial velocity. At any time t and any distance r for the origin, the wave height is described by the function $\eta(r,t)$.

Beginning with the Laplace equation which satisfies the potential function of the flow, and applying the Hankel transform to this equation, then according to a linear theory of waves, $\eta(r,t)$ is given as:

$$\eta(r,t) = -\frac{1}{\rho g^{1/2}} \lim_{y \to o^-} \int_0^\infty s^{3/2} \bar{I}(s)(\tanh sh)^{1/2} \operatorname{sech} sh \times \cosh(y+h) \sin[(gs \tanh sh)^{1/2} t] J_0(rs)\, ds \qquad (1)$$

where s is defined as σ/h. For a derivation of this equation, see Stoker.[2]

In Eq. (1) the function $\bar{I}(s)$ is defined:

$$\bar{I}(s) = \int_0^\infty I(r)\, J_o(sr\, r\, dr \qquad (2)$$

The integral in Eq. (1) is evaluated by use of an asymptotic expansion. It is also necessary to expand the Bessel function by its asymptotic expansion valid for large arguments; i.e.,

$$J_o(x) = \left(\frac{2}{\pi x}\right)^{1/2} \{P_o(x) \cos\left(x - \frac{\pi}{4}\right) - Q_o(x) \sin\left(x - \frac{\pi}{4}\right)\} \qquad (3)$$

where

$$P_o \cong 1 - \frac{1^2 \cdot 3^2}{2!(8x)^2} + \frac{1^2 \cdot 3^2 \cdot 5^2 \cdot 7^2}{4!(8x)^4} - \frac{1^2 \cdot 3^2 \cdot 5^2 \cdot 7^2 \cdot 9^2 \cdot 11^2}{6!(8x)^6} + \ldots$$

$$Q_o \cong -\frac{1^2}{1!(8x)} + \frac{1^2 \cdot 3^2 \cdot 5^2}{3!(8x)^3} - \frac{1^2 \cdot 3^2 \cdot 5^2 \cdot 7^2 \cdot 9^2}{5!(8x)^5} + \ldots$$

Then it is possible to use Kelvin's Stationary phase formula[3] to arrive at Eqs. (4) to (8). In this case, the argument is (rs) and the expansion is valid when r is large, i.e., only in the far field. Instead of using two variables, it is assumed that the ratio r/t is fixed, and then only one large parameter will exist, either r or t. The arguments of the trigonometric functions for the expansion of the Bessel function contain one term which is very large, r, and one which varies more slowly, $s = \sigma/h$. So as s varies slightly, the trigonometric function will go through many oscillations. Assuming that the coefficient in front of the trigonometric functions is somewhat bounded, then the positive areas under the cosine curve will be cancelled by the negative areas when the integral is taken from zero to infinity. However, there may be some places where the oscillation is much slower, and the cancellation will not be complete. These points can be shown to occur when a zero of one of the derivatives of s occurs within the limits of integration.

s is expanded about that point, and the coefficient of the trigonometric function is evaluated at the point. Another important element to be noted is that the sine is rewritten in terms of the cosine, and it is possible to write

$$\int_0^\infty \cos(\text{arg}) = \frac{1}{2}\left[\int_0^\infty \cos(\text{arg}) + \int_{-\infty}^0 \cos(\text{arg})\right]$$

due to the fact that the cosine is an even function.

The following formulas govern the cylindrically symmetric surface waves:

$$\eta(r,t) \sim \frac{I_o R^{1/2}}{\rho g^{1/2} r} A \sin 2\pi \left(\frac{t}{T} - \frac{r}{\lambda}\right) \quad \text{for } r \gg R \tag{4}$$

where

$$\lambda = \frac{2\pi h}{\sigma} \tag{5}$$

$$T = \frac{2\pi}{\left(\frac{g\sigma}{h}\tanh\sigma\right)^{1/2}} \tag{6}$$

$$A = \begin{cases} -\dfrac{\sigma}{I_o R^{1/2} h^{3/2}} \left(\dfrac{\phi(\sigma)\tanh\sigma}{-\phi'(\sigma)}\right)^{1/2} \overline{I}\left(\dfrac{\sigma}{h}\right), & r \le (gh)^{1/2} t \\ 0, & r > (gh)^{1/2} t \end{cases} \tag{7}$$

and the dimensionless auxiliary ϕ is given by

$$\phi(\sigma) \equiv \frac{1}{2}\left(\frac{\tanh\sigma}{\sigma}\right)^{1/2} + \frac{1}{2(\cosh\sigma)^{3/2}}\left(\frac{\sigma}{\sinh\sigma}\right)^{1/2} = \frac{r}{(gh)^{1/2} t} \tag{8}$$

and σ itself is a dimensionless auxiliary variable. The sign $\sim$ has been used to indicate "asymptotically equal to."

In Eqs. (4) to (8), I_o is the initial impulse, R is the effective radius of the impulse, ρ is the density, g is the gravity constant,

r is the distance from the origin, t is the time, A is the variable portion of the amplitude of the wave envelope, T is the period, λ is the wave length, h is the depth of the medium, and $\bar{T}$ is given by Eq. (2).

It should be noted that Eq. (7) is Eq. (2.5) of the Kranzer and Keller paper except for the σ in Eq. (7). This sigma is consistent with Kranzer and Keller's Eq. (2.11) and also agrees with Eq. (B.1) of a paper written by Kriebel.[4] There exist other errors in the original Kranzer and Keller paper which were suspected and later verified by the Kriebel paper. The graphs which are given as Figs. 1, 2, and 3 display $|A|$, $\phi(\sigma)$, and $[\tanh \sigma\, \phi(\sigma)/- \phi'(\sigma)]^{1/2}$. These diagrams are taken from the Kriebel paper, although they are also found in the Kranzer and Keller report. However, Fig. 1 differs from the corresponding graph in Kranzer and Keller. In the Kranzer and Keller paper the maximum value of A is calculated incorrectly, and the labels on the graphs do not indicate correctly what is actually being plotted.

The function $\eta(r,t)$ given by Eq. (4) could be dissected into several portions. First is the term $I_o R^{1/2}/\rho g^{1/2}$, which is a constant. It is obvious that the wave height should be proportional to the magnitude of the initial impulse. It is also proportional to the square root of the effective radius of the initial impulse, but it should be remembered that in the far field the initial impulse will be seen as a point source. Therefore, as r increases, the initial impulse is seen to be more and more like a point source. $\eta(r,t)$ is seen to be inversely proportional to ρ and g. Certainly increasing either ρ or g would cause an increase in the force against the upward displacement of the medium.

Secondly, consider the inverse proportionality to the radius r. The amount of energy in the entire system is fixed by the energy contained in the initial impulse. As the wave moves out radially, this energy is spread out over greater areas. Its intensity diminishes, and so the wave height decreases accordingly.

The varying amplitude factor A is defined in Eq. (7). It depends on the ratio $r/(gh)^{1/2}t$, as seen by comparing Eq. (8) and Eq. (7). If $r > (gh)^{1/2}t$, then A is seen to be zero. This follows from the fact that the maximum group velocity of any wave is $(gh)^{1/2}$. A plot of $|A|$ is given in Fig. 1.

Inspection of Eq. (7) indicates that A is dependent on the initial distribution of impulse $\overline{I}(\sigma/h)$, the effective radius R, and the depth h. All three must be specified for a particular case. Figure 1 plots $|A|$ versus

$$\frac{1}{\phi} = \frac{(gh)^{1/2}\, t}{r}$$

for a parabolic impulse

$$\frac{I(r)}{I_o} = \left[1 - \frac{1}{2}\left(\frac{r}{R}\right)^2\right] \qquad \text{for } r \leq 2^{1/2} R$$

$$= 0 \qquad \text{for } r > 2^{1/2} R$$

So at $r = 0$,

$$\frac{I(r)}{I_o} = 1$$

and at

$$r = (2)^{1/2} R, \quad \frac{I(r)}{I_o} = 0 \quad .$$

The effective radius R is taken as $(2/7)h$ and h is taken as 5 kilometers. These were the values used by Kranzer and Keller for their

examples. Within their paper there are three graphs of $\eta(r,t)$ versus r or versus t (Figs. 4 and 5) for the above specified values of R, h, and initial impulse, where $I_o = 5 \times 10^7$ dyne/sec/cm^2. These same values were used initially in the project in order to verify that the computer program was working properly. By comparing the graphical display of the computer output to the Kranzer and Keller plots it was found that although the graphs had very similar amplitudes and wavelengths, there were some discrepancies. This may be due to the missing σ in their Eq. (2.5), as already mentioned. However, their Eq. (2.11) does include this σ. The second paragraph of Page 401 of their report shows that they wanted to plot $A[r/(gh)^{1/2} t]$ on the abscissa.* The maximum value of $|A|$ given by their Fig. 3 and Table 1 of $A_{max} = .68$ is incorrect in any event.

The computer program gave a maximum value of A as approximately .96, and this was the same value reported in Kriebel's paper. Therefore, the graphs given later in this report, which have the same initial impulse, distances or times that Kranzer and Keller indicated in their Figs. 4 and 5 are to be taken as correct.

The remaining term in Eq. (4), $\sin 2\pi[(t/T) - (r/\lambda)]$, is the portion of the wave height function which causes the more rapid oscillation of the wave height. The varying amplitude A acts as an envelope for this more rapid oscillation. This is easily seen in the plots of $\eta(r,t)$. Both the period T and the wavelength λ are dependent on the dimensionless ratio $r/(gh)^{1/2} t$. T and λ are not fixed constants, so the argument of the sine varies in a complex manner. When $r/[(gh)^{1/2} t] = 1$, then $\phi(\sigma) = 1$ and

---

*This refers to Fig. 3, which is also labeled correctly on the ordinate, but the caption in the graph indicates its inverse.

$$\lim_{\sigma \to 0} \frac{1}{2} \left(\frac{\tanh \sigma}{\sigma} \right)^{1/2} + \frac{1}{2(\cosh \sigma)^{3/2}} \frac{(\sigma)^{1/2}}{(\sinh \sigma)^{1/2}} = 1$$

So when $\sigma = 0$, then

$$\lambda = \frac{2\pi h}{\sigma} \to \infty$$

and

$$T = \frac{2\pi}{\left(\frac{g\sigma}{h} \tanh \sigma \right)^{1/2}} \to \infty \quad .$$

$r[(gh)^{1/2} t] = 1$ corresponds to the outermost part of the wave motion. Therefore, the wavelength and period will be infinite at the extremeties of the wave pattern. Both T and λ will decrease as r decreases for a fixed t, or when t increases for a fixed r. It is to be expected that T and λ should increase near the outer portions of the wave motion. This is because the wave can be considered as many different components which emanate from the origin at constant but at many different speeds. Since the faster portions will form the outermost section of the wave motion, T and λ should be greatest there. This follows from the fact that the speed of a wave varies proportionally with its wavelength and period.

From the above discussion it is clear that the wave pattern expands as it propagates. The amount of this spreading out is proportional to t or to r. For example, for a given t, and considering the wave along one ray, the distance that the wave pattern occupies at large r is much greater than at small r.

It should be noted that $A = 0$ for $[r/(gh)^{1/2}t] > 1$. As mentioned earlier, $r[(gh)^{1/2} t] = 1$ determines the outermost portion of the wave motion, as at distances or times which satisfy $[r/(gh)^{1/2} t] > 1$, the

amplitude of the wave must be zero. $[r/(gh)^{1/2}\ t] > 1$ corresponds to $\phi > 1$.

Looking at Fig. 1, it is seen that $|A|$ goes through several maxima. Had the scale been continued to $1/\phi \to \infty$, there would have been an infinite number of maxima. The distance between the maxima is increasing, and this is due to the aforementioned spreading out of the wave pattern. It is a linear dependence on either t or r which determines this distance between the maxima because ϕ varies linearly with r and t, as seen by Eq. (8). (It should be noted that the σ which satisfies Eq. (8) is the unique non-negative root of that equation). The actual value for the maximum of A will be discussed later.

Consider now the initial impulse distribution. In this project the initial impulse distribution is parabolic in nature and is mathematically described by

$$\frac{I(r)}{I_o} = \left[1 - \frac{1}{2}\left(\frac{r}{R}\right)^2\right] \qquad \text{for } r \leq 2^{1/2} R$$

$$= 0 \qquad \text{for } r > 2^{1/2} R$$

Since in the examples used $h = 5$ kilometers and $R = (2/7)h$, then $R = 1.429$ kilometers. A plot of $I(r)/I_o$ is shown in Fig. 4. It should be noted that at the value $r = R$, the impulse has the value $[I(r)/I_o] = .50$. The effective radius is defined by

$$\frac{1}{2}\,|I_o|\,R^2 = \int_0^\infty r\,|I(r)|\,dr \quad .$$

Then $\pi|I_o|R^2$ is the value of the total initial impulse, and I_o is the maximum value of the impulse distribution.

In order to compute A from Eq. (7), it is necessary to know the value of $\overline{I}(\sigma/h)$ where

$$\bar{I}\left(\frac{\sigma}{h}\right) = \int_0^\infty I(r)\, J_0\left(\frac{\sigma r}{h}\right) r\, dr \quad ,$$

i.e., $\bar{I}(\sigma/h)$ is the zero order Hankel transform of $I(r)$. It is possible to reduce the integral as follows:

$$\frac{\bar{I}(\sigma/h)}{I_0} = \int_0^\infty \frac{I(r)}{I_0} J_0\left(\frac{\sigma r}{h}\right) r\, dr \qquad \text{(i)}$$

$$\frac{I}{I_0} = \left[1 - \frac{1}{2}\left(\frac{r}{R}\right)^2\right] \qquad \text{for} \quad r \le \sqrt{2}\, R$$

$$= 0 \qquad \text{for} \quad r > \sqrt{2}\, R$$

so integral (i) becomes

$$\frac{\bar{I}(\sigma/h)}{I_0} = \int_0^{\sqrt{2}R} \left[1 - \frac{1}{2}\left(\frac{r}{R}\right)^2\right] J_0\left(\frac{\sigma r}{h}\right) r\, dr + \int_{\sqrt{2}R}^\infty 0\, dr$$

$$= \frac{h^2}{\sigma^2} \int_0^{\sqrt{2}R} J_0\left(\frac{\sigma r}{h}\right)\left(\frac{\sigma r}{h}\right) dr \left(\frac{\sigma}{h}\right)$$

$$- \frac{1}{2R^2} \int_0^{\sqrt{2}R} r^3 J_0\left(\frac{\sigma r}{h}\right) dr \qquad \text{(ii)}$$

Recall the relationships

$$\int x\, J_0(x)\, dx = x\, J_1(x)$$

$$\int x^m J_0(x)\, dx = x^m J_1(x) + (m-1)\, x^{m-1} J_0(x)$$

$$- (m-1)^2 \int x^{m-2} J_0(x)\, dx$$

Equation (ii) becomes

$$\frac{I}{I_o} = \frac{h}{\sigma}\sqrt{2}\,R\,J_1\left(\frac{\sigma\sqrt{2}\,R}{h}\right) - \frac{h^3(h)}{2R^2\,\sigma^3(\sigma)}\int_o^{\sqrt{2}\,R}\frac{\sigma^3 r^3}{h^3}J_o\left(\frac{\sigma r}{h}\right)dr\left(\frac{\sigma}{h}\right)$$

$$= \frac{h}{\sigma}\sqrt{2}\,R\,J_1\left(\frac{\sigma\sqrt{2}\,R}{h}\right) - \frac{h^3(h)}{2R^2\,\sigma^3(\sigma)}\left[\frac{r^3\sigma^3}{h^3}J_1\left(\frac{\sigma r}{h}\right)\right.$$

$$\left. + 2\frac{\sigma^2 r^2}{h^2}J_o\left(\frac{\sigma r}{h}\right) - 4\frac{h}{\sigma}\int\frac{\sigma r}{h}J_o\left(\frac{\sigma r}{h}\right)dr\left(\frac{\sigma}{h}\right)\right]_o^{\sqrt{2}\,R}$$

$$\frac{I}{I_o} = \frac{h}{\sigma}\sqrt{2}\,R\,J_1\left(\frac{\sigma\sqrt{2}\,R}{h}\right) - \frac{h^3\,2\sqrt{2}\,R^3\sigma^3\,h}{2R^2\,\sigma^3\,h^3\,\sigma}J_1\left(\frac{\sigma\sqrt{2}\,R}{h}\right)$$

$$- \frac{2h^3\,\sigma^2\,2R^2\,h}{2R^2\,\sigma^3\,h^2\,\sigma}J_o\left(\frac{\sigma\sqrt{2}\,R}{h}\right) + \frac{4\sigma\sqrt{2}\,R\,h^3\,h}{\sigma\,h\,2R^2\,\sigma^3}J_1\left(\frac{\sigma\sqrt{2}\,R}{h}\right)$$

$$\frac{I}{I_o} = \frac{h}{\sigma}\sqrt{2}\,R\,J_1\left(\frac{\sigma\sqrt{2}\,R}{h}\right) - \frac{h}{\sigma}R\sqrt{2}\,J_1\left(\frac{\sigma\sqrt{2}\,R}{h}\right)$$

$$- \frac{2h^2}{\sigma^2}J_o\left(\frac{\sigma\sqrt{2}\,R}{h}\right) + \frac{2\sqrt{2}\,h^3}{R\,\sigma^3}J_1\left(\frac{\sigma\sqrt{2}\,R}{h}\right)$$

Recall that

$$J_{n-1}(x) = \frac{2n}{x}J_n(x) - J_{n+1}(x)$$

$$\therefore\ J_o(x) = \frac{2}{x}J_1(x) - J_2(x)$$

Then,

$$-\frac{2h^2}{\sigma^2}J_o\left(\frac{\sigma\sqrt{2}\,R}{h}\right) = -\frac{2h\,2h^2}{\sigma^3\sqrt{2}\,R}J_1\left(\frac{\sigma\sqrt{2}\,R}{h}\right)$$

$$+\frac{2h^2}{\sigma^2}J_2\left(\frac{\sigma\sqrt{2}\,R}{h}\right)$$

so,

$$\frac{\bar{I}}{I_o} = -\frac{4h^3}{\sigma^3 \sqrt{2}\, R}\left(\frac{\sqrt{2}}{\sqrt{2}}\right) J_1\left(\frac{\sigma\sqrt{2}\, R}{h}\right) + \frac{2h^2}{\sigma^2} J_2\left(\frac{\sigma\sqrt{2}\, R}{h}\right)$$

$$+ \frac{2\sqrt{2}\, h^3}{R\,\sigma^3} J_1\left(\frac{\sigma\sqrt{2}\, R}{h}\right)$$

$$= -\frac{2\sqrt{2}\, h^3}{\sigma^3 R} J_1\left(\frac{\sigma\sqrt{2}\, R}{2}\right) + \frac{2\sqrt{2}\, h^3}{\sigma^3 R} J_1\left(\frac{\sigma\sqrt{2}\, R}{h}\right)$$

$$+ \frac{2h^2}{\sigma^2} J_2\left(\frac{\sigma\sqrt{2}\, R}{h}\right)$$

Finally,

$$\frac{\bar{I}(\sigma/h)}{I_o} = \frac{2h^2}{\sigma^2} J_2\left(\frac{\sigma\sqrt{2}\, R}{h}\right) \qquad (9)$$

Independent of the shape of the initial impulse distribution is the actual amount of energy that is imparted to the medium. The amplitude A will asymptotically approach zero, as $r/(gh)^{1/2}\, t$ approaches zero, if the amount of energy imparted is finite. The total energy Q is given by the expression

$$Q = \frac{\pi}{\rho} \int_0^\infty \left[\frac{\sigma}{h}\bar{I}\left(\frac{\sigma}{h}\right)\right]^2 \tanh \sigma h \; d(\sigma h) \qquad (10)$$

Of course, in all real situations Q will be finite. Only if I(r) is discontinuous will Q be infinite.

Continuing with the discussion of the parabolic impulse, it is possible to find the maximum values of all the variables. Figure 3 shows that

$$\sqrt{\frac{\tanh \sigma\, \phi(\sigma)}{-\phi'(\sigma)}} \to \sqrt{2}\sqrt{\sigma} \qquad \text{for} \quad \sigma \geq 4 \qquad (A)$$

and for $\sigma > 4$, Fig. 2 shows that $\phi(\sigma) \to \frac{1}{2\sqrt{\sigma}}$

Then

$$\phi^2 = \frac{\sigma}{4} \qquad \text{or} \qquad \sigma = \frac{1}{4\,\phi^2}$$

Since

$$\phi = \frac{r}{(gh)^{1/2}\,t}$$

then

$$\sigma = \frac{gh\,t^2}{4\,r^2} \tag{B}$$

Substituting relationships (A) and (B) into Eq. (7), then

$$A \approx \frac{\sigma\sqrt{2\sigma}\,\bar{I}(\sigma h)}{h\,I_o\sqrt{Rh}} = \frac{\sqrt{2}\,(\sigma)^{3/2}\,(R)^{3/2}\,\bar{I}(\sigma h)}{h^{3/2}\,I_o\,R^2}$$

but,

$$\frac{(\sigma)^{3/2}}{(h)^{3/2}} = \frac{g^{3/2}\,h^{3/2}\,t^3}{4^{3/2}\,r^3\,h^{3/2}} = \left(\frac{gt^2}{4r^2}\right)^{3/2}$$

so the variable h plays no part in determining the amplitude A for $\sigma \geq 4$. Therefore, the depth of the water is important only in the leading portion of the wave envelope, but the frequency of the actual wave is always dependent on h.

Introducing the variable $s = \sigma/h$ then for $\sigma \geq 4$,

$$A = \sqrt{2}\,(Rs)^{3/2}\,\frac{\bar{I}(s)}{I_o\,R^2} \quad ,$$

and s has already been shown to be independent of h for $\sigma \geq 4$. For a parabolic impulse, it has already been proven that

$$\frac{\bar{I}(s)}{I_o\,R^2} = \frac{(2)\,J_2(\sqrt{2}\,Rs)}{(Rs)^2}$$

Then,

$$A \approx \frac{\sqrt{2}\,(Rs)^{3/2}\,(2)\,J_2(\sqrt{2}\,Rs)}{(Rs)^2} = 2\sqrt{2}\,(Rs)^{-1/2}\,J_2(\sqrt{2}\,Rs)$$

Kriebel indicates that at $Rs(= gRt^2/4r^2) = 2.70/\sqrt{2}$, A is at a maximum. At $Rs = 1.91$, $J_2(\sqrt{2}\,Rs) = .473$ and $(Rs)^{-1/2} = \sqrt{1.414}/1.64$. Then $A_{max} = (2.828)(1.414)^{1/2}\,(.286) = .962$. This is the first maximum indicated in Fig. 1.

At $Rs = 1.91$, $R\sigma/h = 1.91$, and at the transition point $\sigma = 4$, $R/h = 1.91/4 = .48$, and $\sqrt{2}\,R = .68h$. So for $Rs \leq 1.91$, the depth h has no effect on the amplitude A. Therefore, if $\sqrt{2}\,R \leq .68h$, then the peak value of A is independent of the depth of the medium. ($\sqrt{2}\,R$ is the actual radius of the initial impulse.)

In summary, the following maximum values exist,

$$A_{max} = .962$$

$$\sigma_{max} = 1.91\ h/R = \frac{ght^2}{4r^2}$$

$$\lambda_{max} = \frac{2}{1.91}\,R = 2.3$$

$$T_{max} = 3.7\,(R/g)^{1/2}$$

$$t_{max} = \sqrt{\frac{7.64}{gR}}\,(r)$$

$$\eta_{max} = \frac{.962\ I_o}{\rho\ r}\sqrt{\frac{R}{g}}$$

Kranzer and Keller also mention other distributions than parabolic ones. Their Table I has been reproduced below. Listed are the maximum values of some of the variables for five different distributions of the initial impulse. Table II and Fig. 5 contain some values for the same distributions

TABLE I. CHARACTERISTICS OF FIVE DIFFERENT DISTRIBUTIONS OF INITIAL IMPULSE (From Kranzer & Keller)

$\frac{I(r)}{I_0}$	$1,\ r\le R$ $0,\ r>R$	$\left[1-\frac{1}{2}\left(\frac{r}{R}\right)^2\right],\ r\le 2^{\frac{1}{2}}R$ $0,\ r>2^{\frac{1}{2}}R$	$\left[1+2\left(\frac{r}{R}\right)^2\right]^{-\frac{1}{2}}$	$e^{-2^{\frac{1}{2}}r/R-1}$	$e^{-(r/R)^2}$
A_{max}	1.1	0.96	0.49	0.42	0.76
$\frac{V_{max}}{(gR)^{\frac{1}{2}}}$	0.33	0.30	0.35	0.42	0.38
$\frac{\lambda_{max}}{R}$	2.8	2.3	3.1	4.4	3.6
$\frac{T_{max}}{(R/g)^{\frac{1}{2}}}$	4.1	3.7	4.3	5.3	4.8
Secondary maxima	Infinitely many; practically constant amplitude	Infinitely many; amplitudes decrease like r^{-2}	None	None	None
$Q/\pi R\rho^{-1}I_0^3$	∞	0.48	0.18	0.14	0.31
$\frac{I(s)}{I_0}(s=\sigma h^{-1})$	$\frac{R}{s}J_1(Rs)$	$\frac{2}{s^2}J_2[2^{\frac{1}{2}}Rs]$	$\frac{1}{2}R^2e^{-Rs/2^{\frac{1}{2}}}$	$\frac{R^2}{2[1+\frac{1}{2}R^2s^2]^{\frac{1}{2}}}$	$\frac{1}{2}R^2e^{-(Rs)^2/4}$

TABLE II (From Kriebel)

I/I_o	A_m Eq. (B.45)	q Eq. (B.44)	$A_m/\sqrt{q}$	$\bar{I}(s)/I_o$ Eq. (B.1)	$-\frac{\rho R}{I_o}v_o$ Table B-1
1	1.16	∞	0	$\frac{R}{s}J_1(Rs)$	∞
2	0.96	0.48	1.39	$\frac{2}{s^2}J_2\sqrt{2}Rs$	$\sqrt{2}$
3	0.49	0.18	1.15	$\frac{R^2}{2}e^{-\frac{Rs}{\sqrt{2}}}$	$2\sqrt{2}$
4	0.42	0.14	1.12	$\frac{R^2}{2}\left(1+\frac{R^2s^2}{2}\right)^{-\frac{3}{2}}$	∞
5	0.76	0.31	1.37	$\frac{R^2}{2}e^{-\left(\frac{Rs}{R}\right)^2}$	$\sqrt{\pi}$

as given by Kriebel. Included in Fig. 5 is a graphical display of the distributions. The parabolic impulse has been labeled as number 2. (Note that V_{max} refers to the group velocity in Table II.)

Among the distributions listed is a discontinuous distribution given by

$$\frac{I(r)}{I_o} = 1 \qquad r \leq R$$

$$= 0 \qquad r > R$$

As a result of the discontinuity, Q is infinite. This causes infinitely many maxima to be generated which do not approach a zero magnitude, and the distance between maxima decreases as t increases. The other four distributions are all continuous and so contain a finite amount of energy. Kranzer and Keller point out that "The last three have no secondary maxima while the first has infinitely many, the magnitudes of which decrease like t raised to the minus 2 power (for fixed r). The existence of secondary maxima and their rate of decrease depend upon the smoothness of I(r). If I(r) is discontinuous infinitely many maxima of practically constant amplitude will occur. If I(r) is continuous but its derivative discontinuous for some $r \neq 0$, infinitely many maxima will occur with amplitudes decreasing like t raised to the minus 2 power (for fixed r). If I(r) and all its derivatives are continuous there are usually only a finite number of maxima, and if I(r) is a decreasing function only one maximum can be expected." (from p. 401).

In the Kriebel paper, the case of very deep water $(h \to \infty)$ is also considered. By examining this situation the effect of changing the effective radius R and the total impulse and total energy can be found.

Previously, in Eq. (10), the quantity Q was defined as the total

energy imparted to the medium. When considering a parabolic distribution, with $h \to \infty$, and using the relationship of Eq. (9), then,

$$\frac{\rho Q}{\pi R I_o^2} = 4 \int_0^\infty \frac{J_2^2(\sqrt{2}\, Rs)\, d(Rs)}{(Rs)^2}$$

$$= \frac{\sqrt{2}}{\Gamma(7/2)\,\Gamma(3/2)} = \frac{16\sqrt{2}}{15\pi} = .480$$

Then,

$$Q = \frac{.480\, \pi\, R\, I_o^2}{\rho}$$

The total impulse was also previously defined and is given by

$$J = \pi R^2 I_o$$

Equation (4) defines $\eta(r,t)$ as

$$\eta(r,t) \sim \frac{I_o R^{1/2}}{\rho g^{1/2} r} A \sin 2\pi \left(\frac{t}{T} - \frac{r}{\lambda} \right)$$

It has been shown that $A_{max} = .962$, and the maximum value of $\sin 2\pi [(t/T) - (r/\lambda)] = 1$. Then,

$$\eta_{max} = \frac{.962\, I_o R^{1/2}}{\rho g^{1/2} r}$$

Therefore, in terms of J and Q,

$$\eta_{max} = \frac{.962\, J}{\pi R^2 \rho r} \sqrt{\frac{R}{g}} = \frac{.962}{r} \sqrt{\frac{Q}{.48\, \rho\, g}}$$

$$\eta_{max} = \frac{.785}{r} \sqrt{\frac{Q}{\rho\, g}}$$

Then for a given total impulse J, η_{max} is proportional to $R^{-3/2}$. For a given Q, η_{max} is inversely proportional to r and is independent of R. (Kriebel points out that the time of the arrival of this maximum wave

height is $t = \sqrt{(7.64/gR)}\, r$, which is dependent on R.)

From Fig. 5 it is seen that as $I(r)$ becomes more peaked, then the value of A_{max}, and therefore η_{max}, decrease. For example, I/I_o of curve 4 is more peaked than curve 2, and A_{max} is almost half as great for curve 4. It must be remembered that all of these curves and all comparisons are made with the same I_o and R. Ans since both J and Q are determined by only these two variables, then the total impulse and total energy in all of these cases is the same.

DISCUSSION OF THE COMPUTER PROGRAM

Using a CDC 7600 computer a program caled WWAVES was written to evaluate the function $\eta(r,t)$. Basically, Eq. (4) was solved using the values calculated in Eqs. (5) - (8).

Kranzer and Keller suggested that a value of ϕ be selected, and then the corresponding values of either r or t calculated from Eq. (8). This was the first method in approaching this project; however, this led to equal increments in ϕ and varying increments in r or t. Since it was desired to later also superimpose the waves resulting from several initial impulses, it was necessary to have equal increments in r or t.

To find equal increments in r (or t), Eq. (8) was solved for σ for a given t (or r). Equation (8) is a transcendental equation in σ and not readily solved. Figure 2 graphs Eq. (8). Consider now a fixed t and r varying. r will be set at some lower limit, which satisfies $r << R$. In order now to solve for σ, Newton's method was first applied. But due to the flatness of Eq. (8) as seen in Fig. 2, this method of root finding was very slowly converging in some regions and even diverging in some areas. Next, the Method of False Position was used with greater success. A schematic

diagram of this portion of the program is found in Fig. 6. It is based on the equation

$$x_{(n+1)} = x_{(n)} + \frac{|f(x_{(n)})|}{|f(x_{(n-1)})| + |f(x_{(n)})|} (x_{(n-1)} - x_{(n)})$$

This schematic is taken from page 10 of An Introduction to Determination of Roots of Equations, by C. D. Mote, Jr. Quoting from page 8 of these notes, "The method (of False Positon) is used to determine a real root x_i of the equation $f(x) = 0$ when values of the function $f(x)$ are known at $x_n = x_i -$ and $x_{(n-1)} = x_i +$. The root is estimated by linearly interpolating between the values of the function (with opposite signs) at successive trial positions.: Graphically:

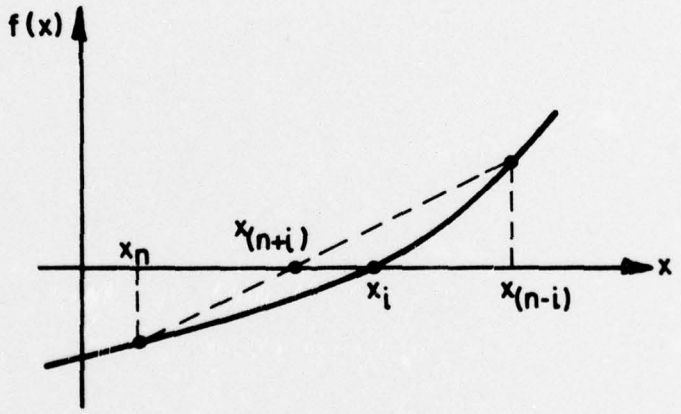

The disadvantage of using the method of false position is that the root must be between two known values. Therefore, values of σ were pre-selected between which the root value of σ was definitely known to lie. This restriction and the flatness of the equation caused slow convergence. The method of false position is an iterative one, and the test for convergence was set to a pre-selected tolerance. For all of the output in

this report the error criteria is .01. Greater accuracy is easily available, but involves more computer time.

Once σ was found, it was substituted into Eqs. (5), (6), and (7), and these resulting values allowed $\eta(r,t)$ to be calculated. Then the value of the varying variable was incremented and the cycle started over again.

Next the maximum and minimum values of $\eta(r,t)$ and either r or t were found. The general form of the printed program can be found later in this report.

Now it is possible to use the Graphical Display System (GDS) which is in the computer library to plot $\eta(r,t)$. The necessary parameters for the plot are set and the graph is printed on the line printer. The GDS file is then disposed to microfiche, which gives a fine line plot. Only microfiche copies of the output are found within this report. The subroutine available in the GDS library is entitled PFLILI. It utilizes a parabolic fairing technique to draw a curve through a set of points. Therefore, the plot of $\eta(r,t)$ is a very smooth curve and not a series of straight lines. Also included in the plot is the wave envelope, indicated by dotted lines.

This section of the report includes several cases of initial impulse distribution. The first case includes the computer output partially showing the digital results. The corresponding plot graphically displays the wave height versus time for three initial impulses. The resulting waves from the initial impulses have been superimposed. It should be noted that since the size of the graph on the vertical axis is constant for all the graphs, it is possible to compare wave heights between different cases only by comparing their actual value and not their height on the graph. Since it is possible to superimpose several waves, a study of the waves resulting

from actual impulses, rather than idealized parabolic ones, can be undertaken.

The next six plots display wave height versus time for one particular initial impulse while the distance from the impulse has been varied. Note that the wave envelope spreads out as the distance from the impulse changes from 20 to 30 kilometers.

The next set of graphs are of wave height versus distance with time varying from 350 to 500 seconds. As the time from the initial impulse is increased, the wave envelope can be seen to be spreading.

Finally, the last two pages contain a comparison between empirical data, and information generated by the computer program. Full information for the actual tests was not available, so it is impossible to fully compare the theoretical with the actual results. In the second of the two experiments cited, the depth of the water was not given, but was assumed to be 130 feet (an approximation for deep water). This approximation may have caused the discrepancy in the frequencies. It should be noted that in the first graph presented the wave does not touch the wave envelope. This is due to the low number of data points that the computer was able to generate. It is felt that what is really important to gain from this graph is the value of the maximum of the wave envelope. This also applies to the second graph, although more resolution could have been obtained had the program been instructed to generate more data points. It was felt that the time and expense involved was not necessary. In general, it can be concluded that there was fairly good correlation between the empirical data and the wave shapes predicted by Kranzer and Keller's theory.

REFERENCES

1. H. C. Kranzer and J. B. Keller, "Water Waves Produced by Explosions," J. Applied Phys. 30, 3, 398-407, 1959.

2. J. J. Stoker, Water Waves, Interscience Publishers, Inc., New York, 1958, Secs. 6.4 and 6.5.

3. Sir W. Thomson, Proc. Roy. Soc. (London) A43, 80 (1887), Papers IV, 303.

4. A. R. Kriebel, Analysis of Water Waves Generated Explosively At the Upper Critical Depth, URS Corp., 1968.

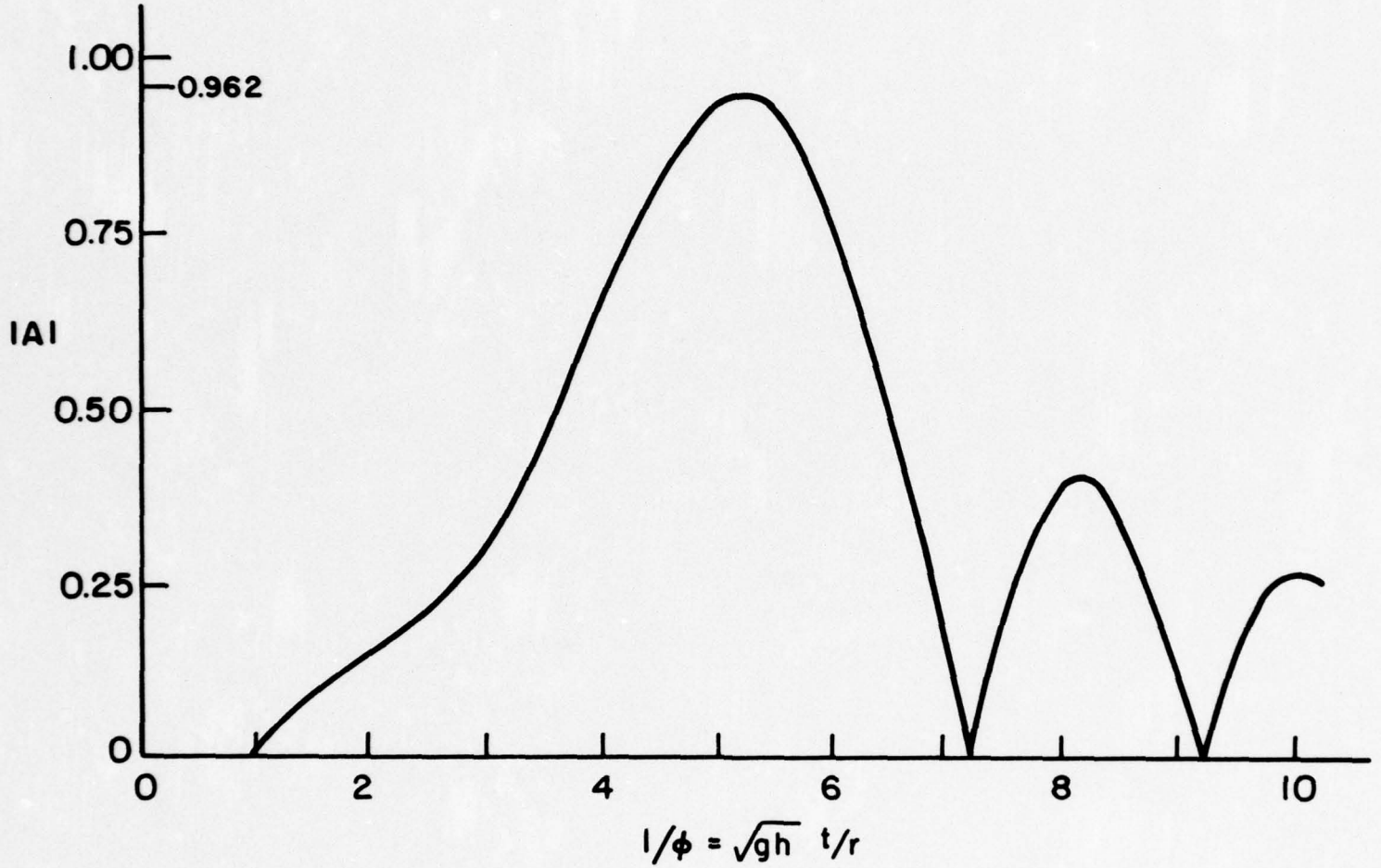

FIG. 1. |A| versus $1/\phi$ FOR A PARABOLIC IMPULSE, R = (2/7)h, h = 5 KM, and $I_o = 5 \times 10^7$ dyne sec/cm^2 (from Kriebel)

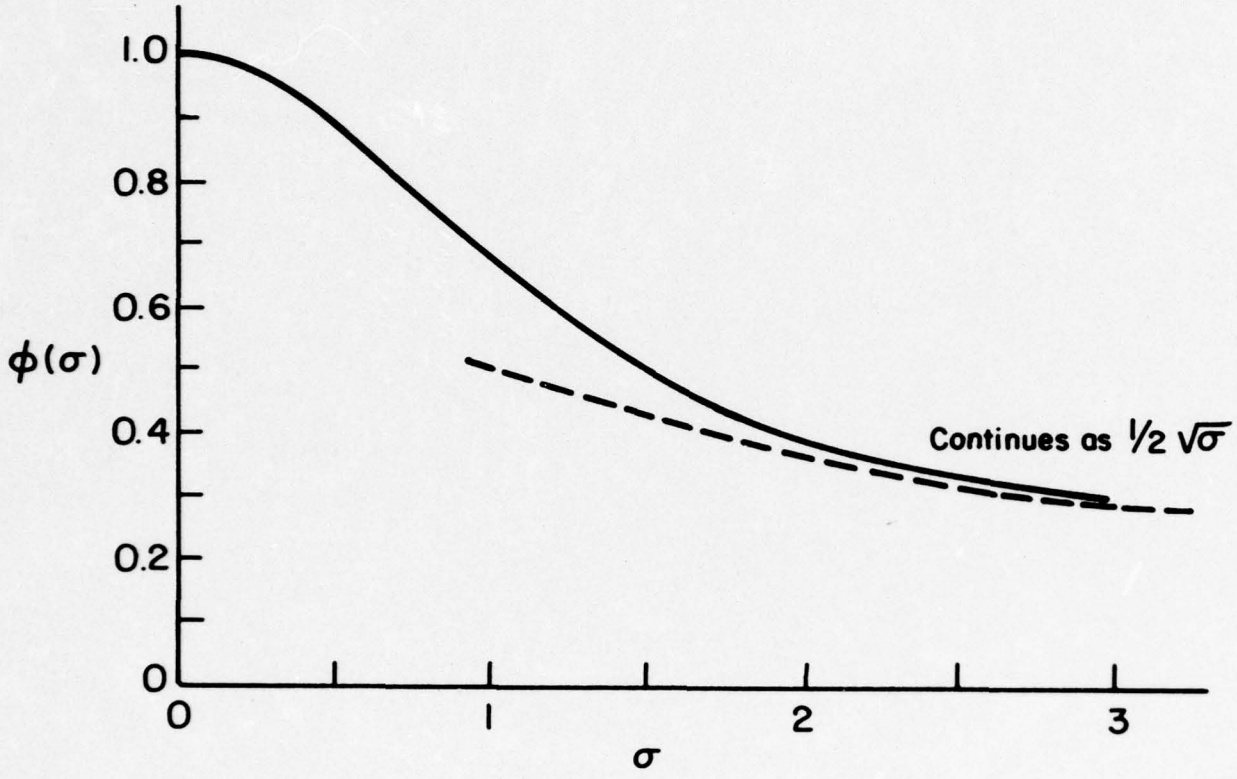

FIG. 2. $\phi(\sigma) = 1/2 \left(\frac{\tanh \sigma}{\sigma} \right)^{1/2} + 1/2(\cosh \sigma)^{-3/2} \left(\frac{\sigma}{\sinh \sigma} \right)^{1/2} = \frac{r}{\sqrt{gh}\, t}$

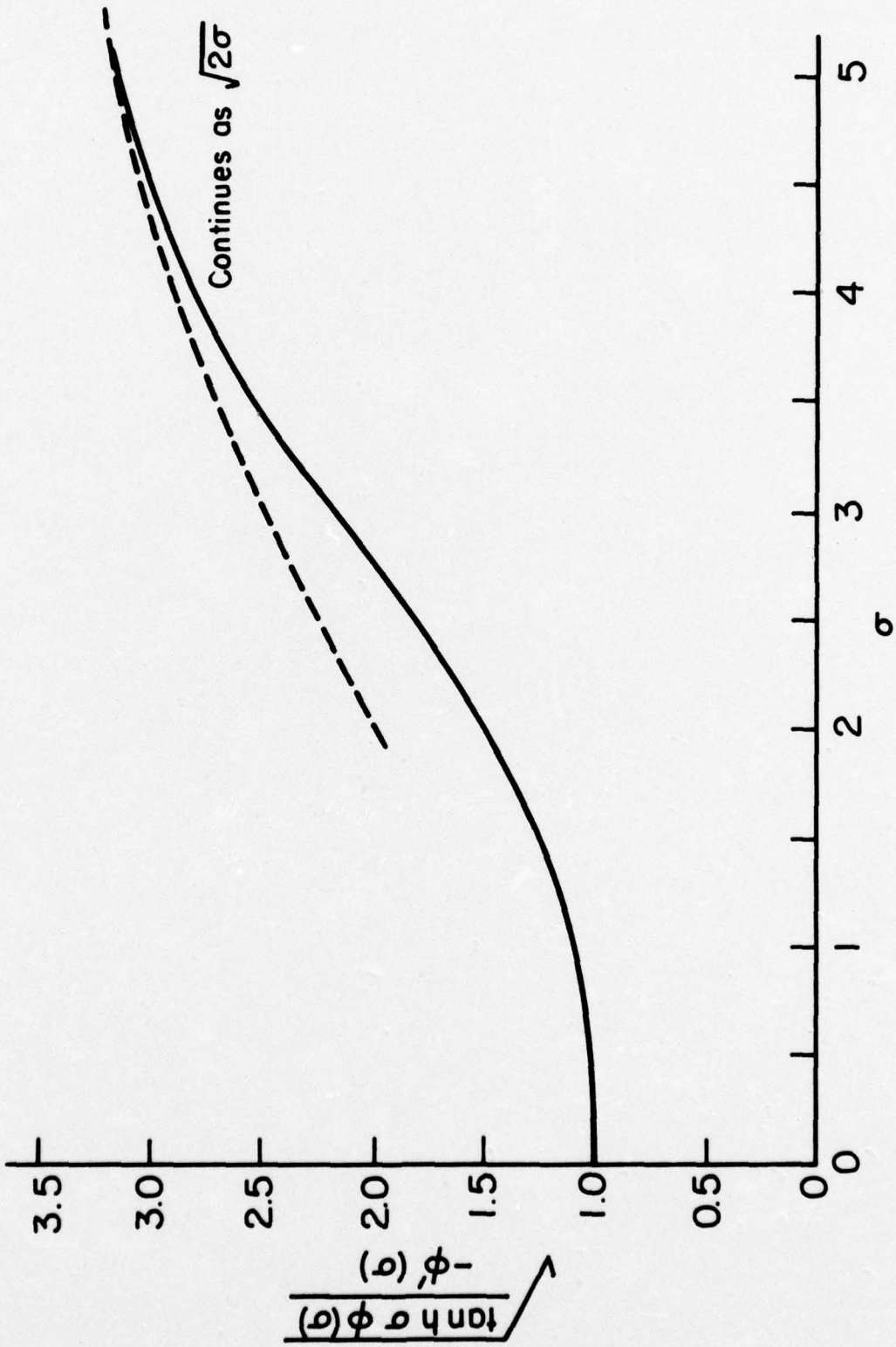
Continues as $\sqrt{2\sigma}$
$\frac{\tanh \sigma \phi(\sigma)}{-\phi'(\sigma)}$
3.5
3.0
2.5
2.0
1.5
1.0
0.5
0
0
1
2
3
4
5
σ

FIG. 3.

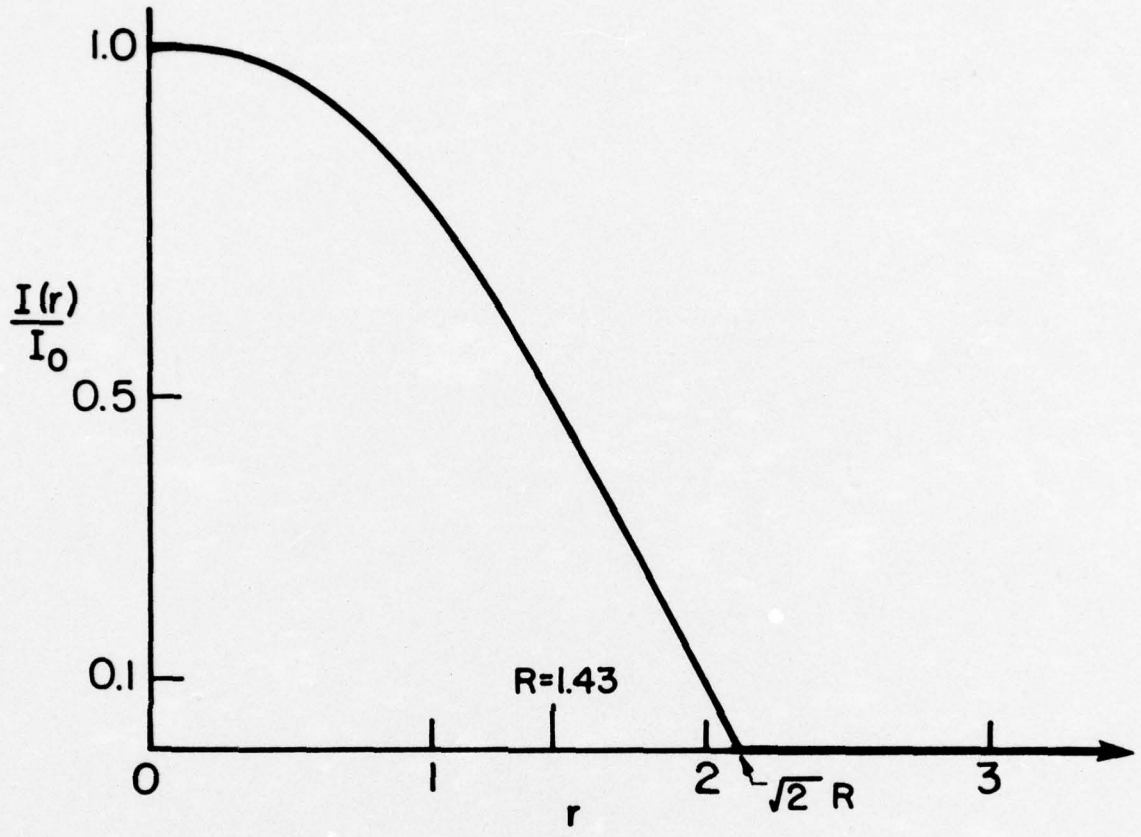

FIG. 4. $I(r)/I_o$ versus r FOR A PARABOLIC DISTRIBUTION

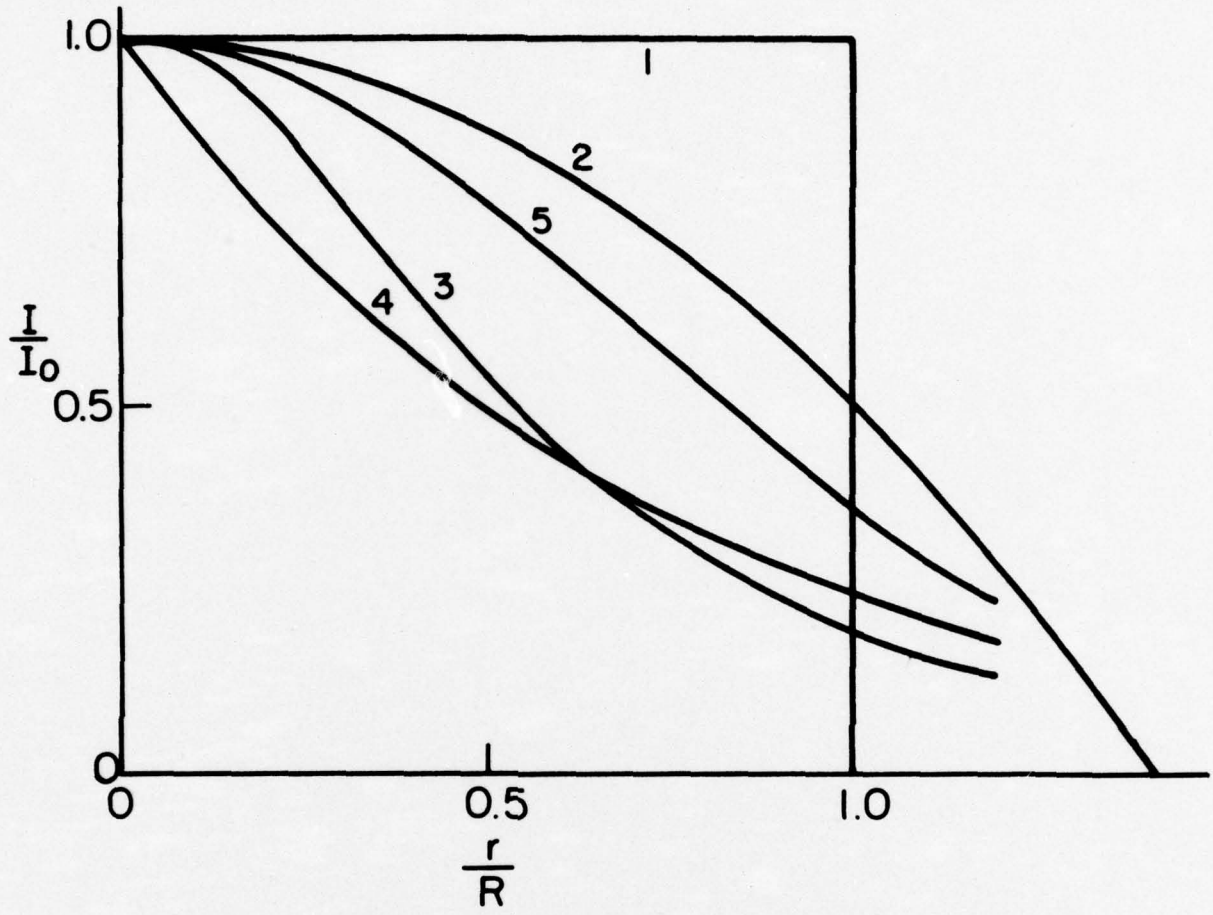

FIG. 5. IMPULSE DISTRIBUTIONS (from Kranzer and Keller)

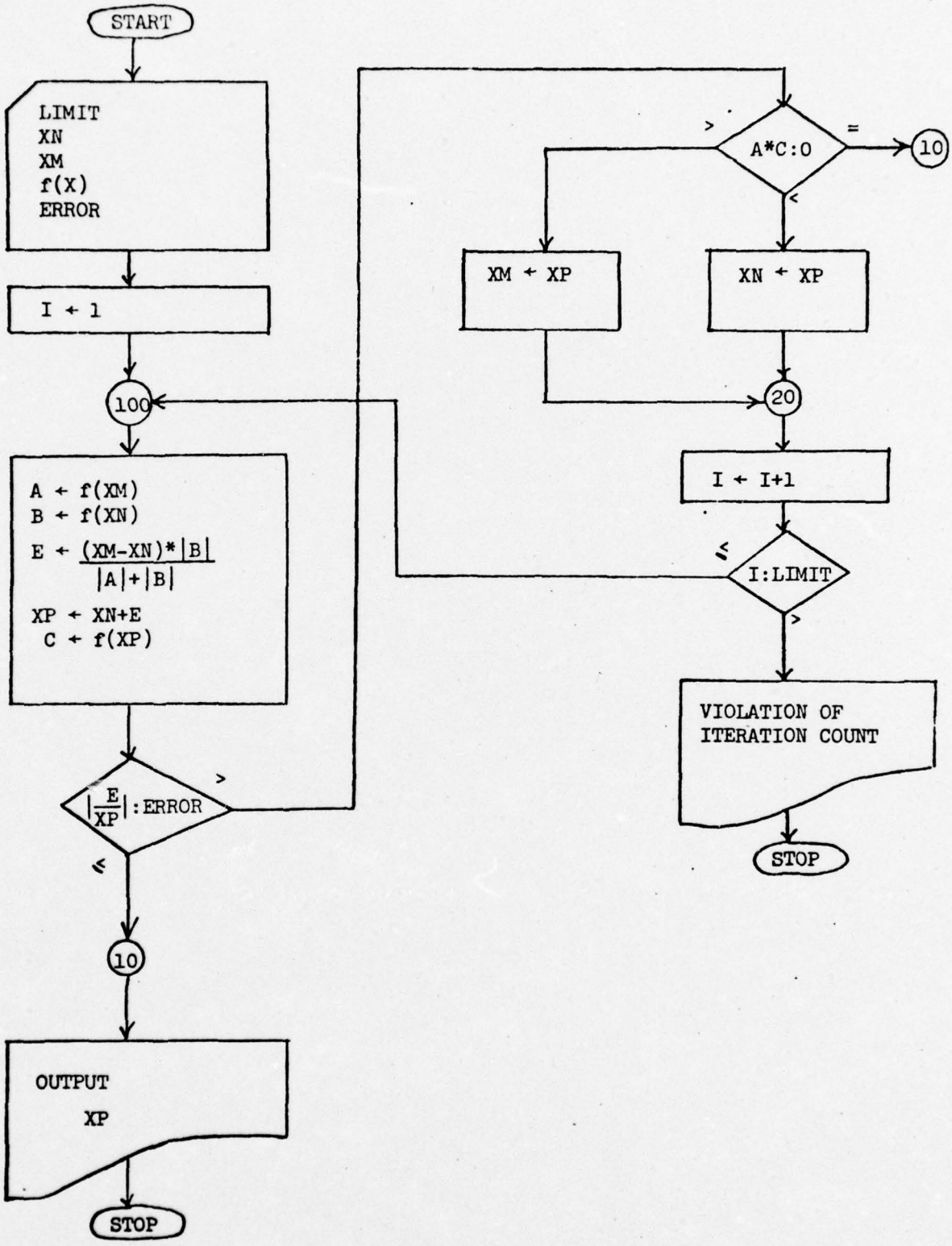

FIG. 6. FALSE POSITION COMPUTER FLOW DIAGRAM

THIS OUTPUT REPRESENTS THE WATER WAVES GENERATED BY AN INITIAL IMPULSE WITH THE FOLLOWING DISTRIBUTION

INITIAL IMPULSE (DYNES-SEC/CM2)	PHASE SHIFT (SEC)
5.000E+07	0.
4.250E+07	.0100
3.500E+07	.0200

THE DENSITY OF THE MEDIUM WAS TAKEN AS 1.025 GR/CM3

THE DISTANCE FROM THE IMPULSE FOR THIS DATA IS 26.000 KILOMETERS

THE DEPTH OF THE MEDIUM IS 5.000 KILOMETERS

THE EFFECTIVE RADIUS OF THE IMPULSE IS 1.429 KILOMETERS

DISPALCEMENT (METERS)	TIME (SEC)	DISTANCE (KM)	ENVELOPE (METERS)
0.	100.010	26.000	0.
0.	105.020	26.000	0.
0.	110.030	26.000	0.
0.	115.040	26.000	0.
-.001	120.050	26.000	-.023
-.012	125.060	26.000	-.161
-.035	130.070	26.000	-.209
-.068	135.080	26.000	-.250
-.112	140.090	26.000	-.287
-.164	145.100	26.000	-.320
-.223	150.110	26.000	-.352
-.286	155.120	26.000	-.382
-.349	160.130	26.000	-.412
-.409	165.140	26.000	-.441
-.460	170.150	26.000	-.469
-.497	175.160	26.000	-.497
-.515	180.170	26.000	-.525
-.508	185.180	26.000	-.552
-.474	190.190	26.000	-.580
-.409	195.200	26.000	-.608
-.313	200.210	26.000	-.636
-.197	205.220	26.000	-.665
-.035	210.230	26.000	-.693
.136	215.240	26.000	-.723
.316	220.250	26.000	-.752
.494	225.260	26.000	-.782

.153	1472.750	26.000	-.863
.901	1477.760	26.000	-.901
.160	1482.770	26.000	-.929
-.891	1487.780	26.000	-.946
-.461	1492.790	26.000	-.952
.745	1497.800	26.000	-.946
.678	1502.810	26.000	-.929

THE MAXIMUM OF THE ABSOLUTE VALUE OF ETA IS 5.492E+00 METERS

THE MAXIMUM OF THE ABSOLUTE VALUE OF THE WAVE ENVELOPE AMPLITUDE IS 5.551E+00 METERS

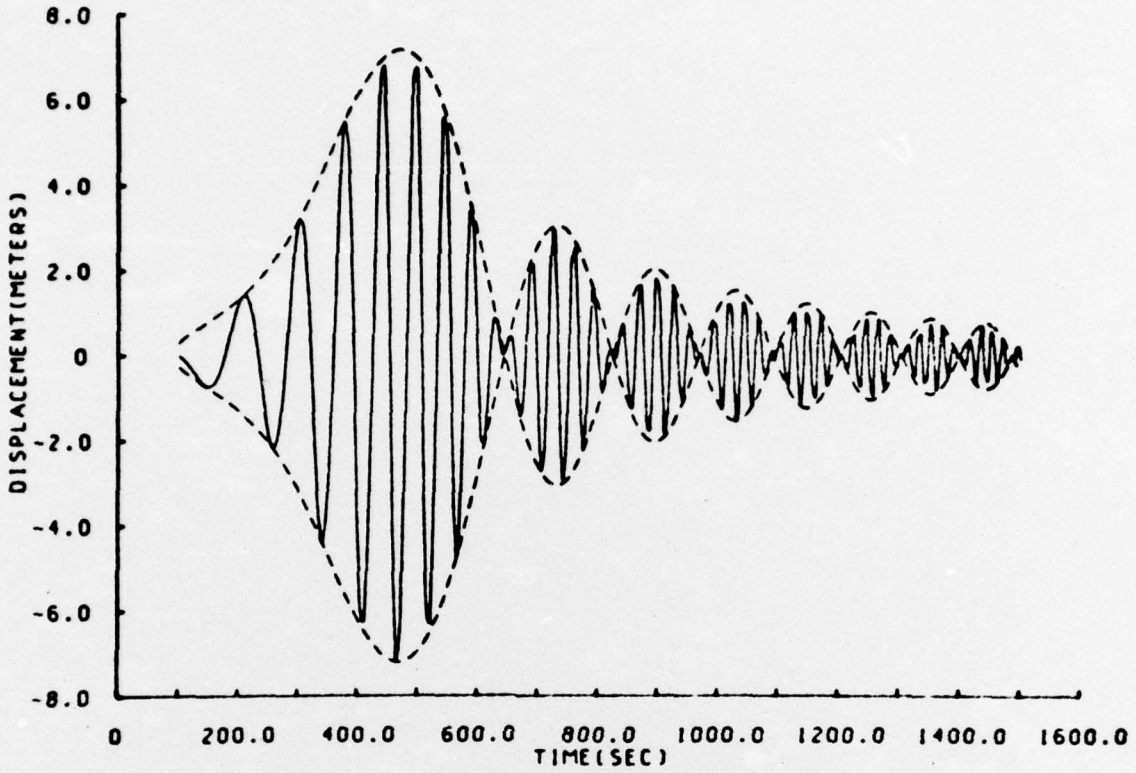

PLOT OF ETA VERSUS TIME

INITIAL IMPULSE(DYNE-SEC/CM2)	DISTANCE(KM)	PHASE SHIFT
50000000.00	20.00	.0000
42500000.00		.0100
35000000.00		.0200

FIG. 7.

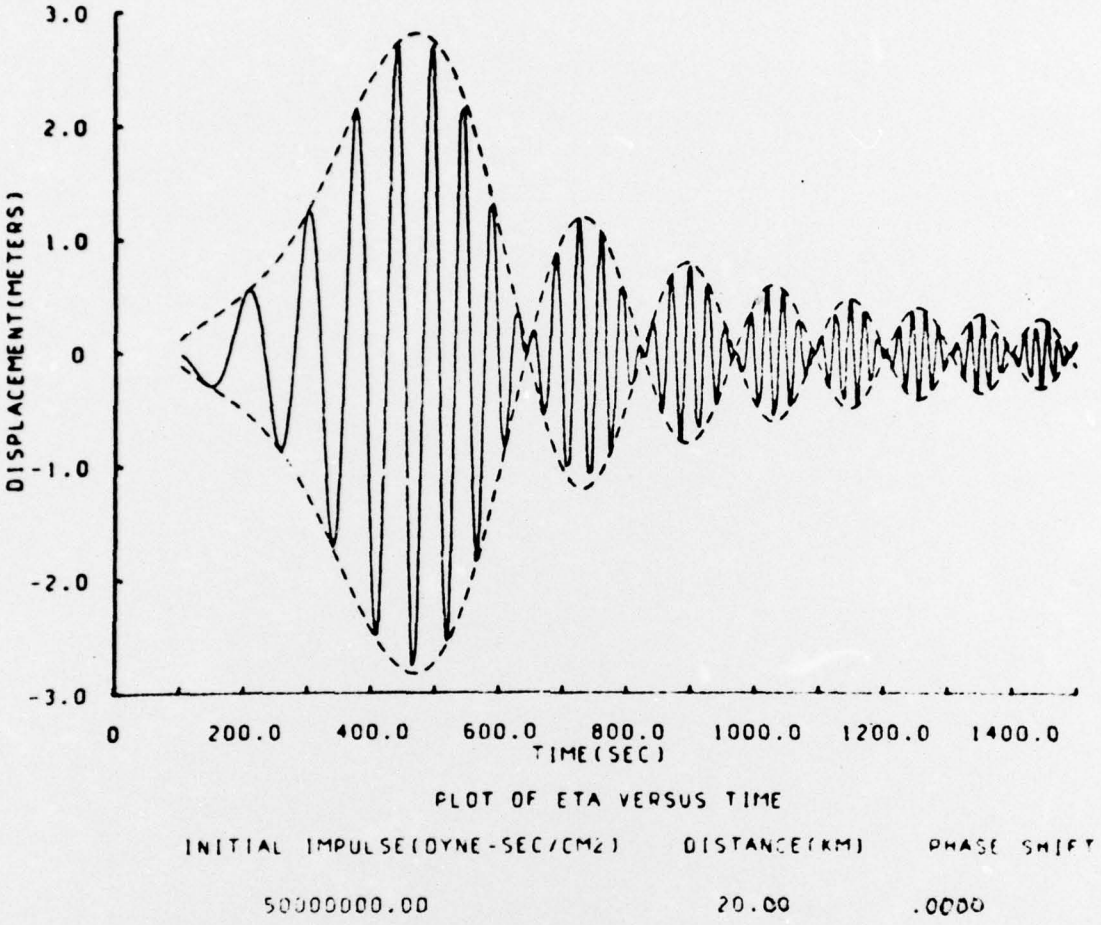
3.0
2.0
1.0
0
-1.0
-2.0
-3.0
DISPLACEMENT(METERS)
0
200.0
400.0
600.0
800.0
1000.0
1200.0
1400.0
TIME(SEC)
PLOT OF ETA VERSUS TIME
INITIAL IMPULSE(DYNE-SEC/CM2)
DISTANCE(KM)
PHASE SHIFT
50000000.00
20.00
.0000

FIG. 8.

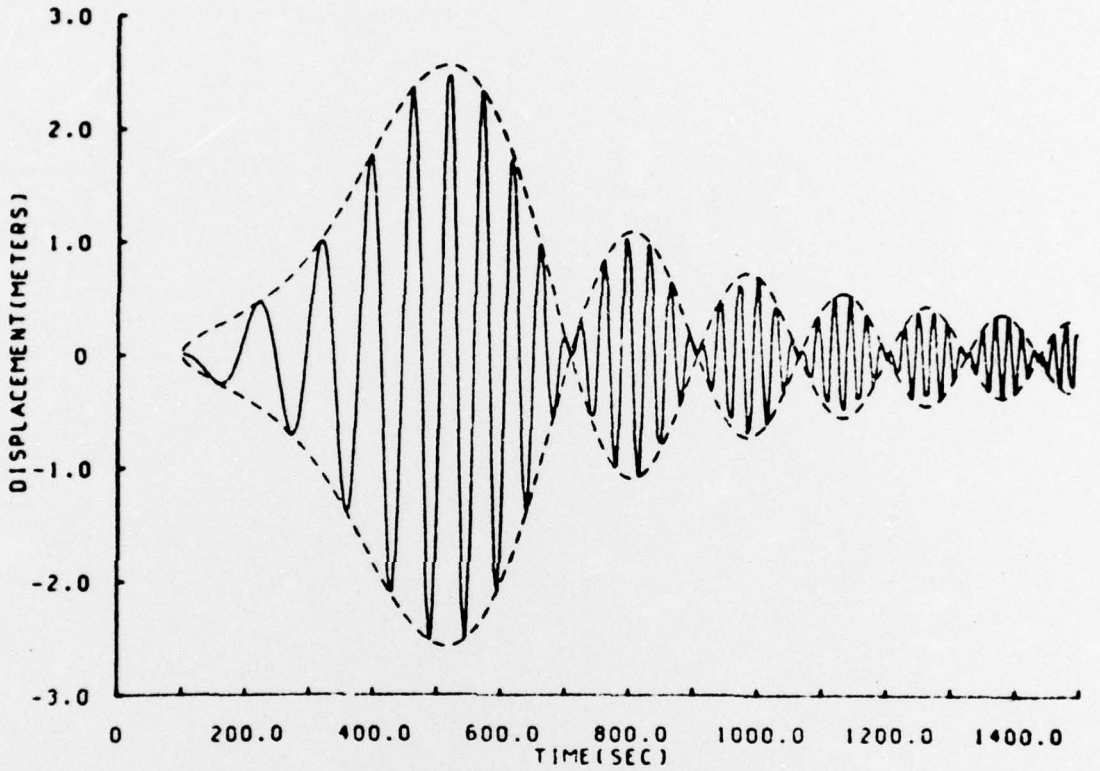
3.0
2.0
1.0
0
-1.0
-2.0
-3.0
DISPLACEMENT(METERS)
0
200.0
400.0
600.0
800.0
1000.0
1200.0
1400.0
TIME(SEC)
PLOT OF ETA VERSUS TIME
INITIAL IMPULSE(DYNE-SEC/CM2)
DISTANCE(KM)
PHASE SHIFT
50000000.00
22.00
.0000

FIG. 9.

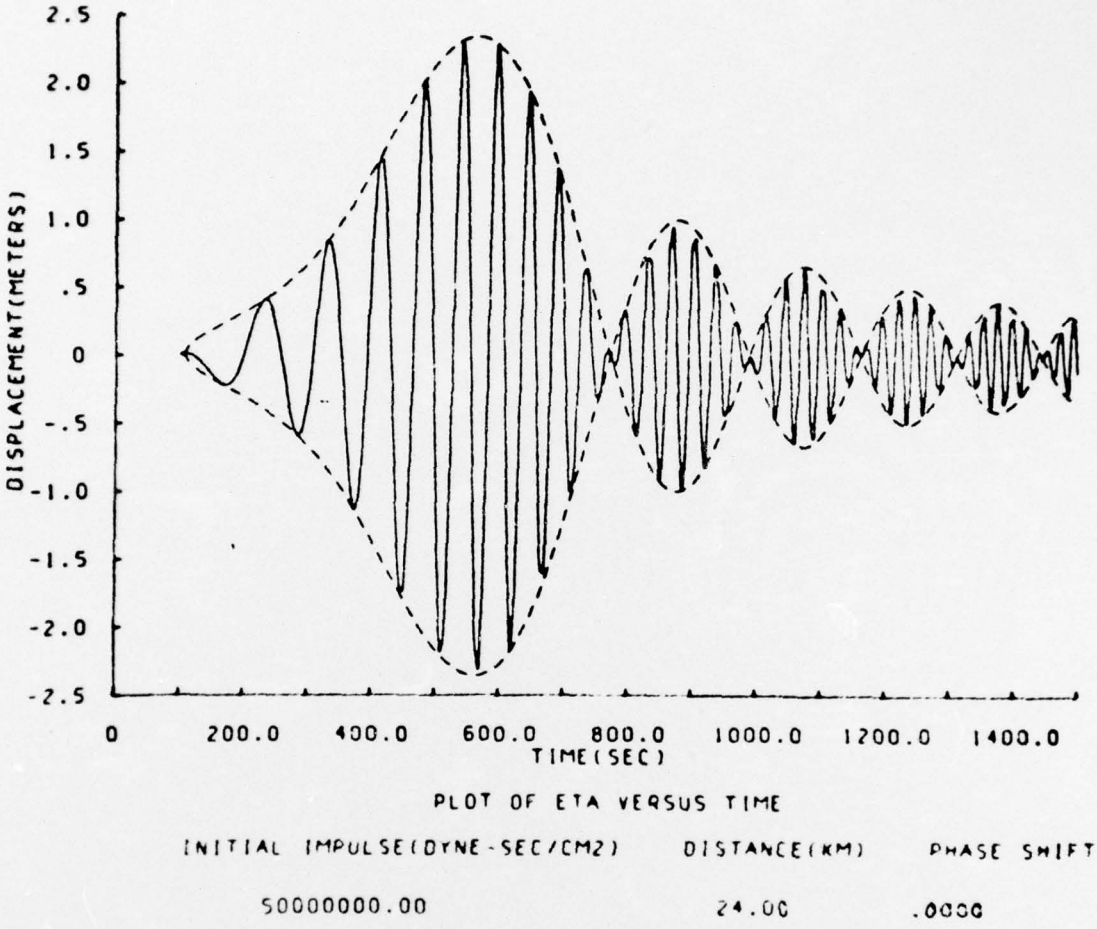
2.5
2.0
1.5
1.0
.5
0
-.5
-1.0
-1.5
-2.0
-2.5
DISPLACEMENT(METERS)
0
200.0
400.0
600.0
800.0
1000.0
1200.0
1400.0
TIME(SEC)
PLOT OF ETA VERSUS TIME
INITIAL IMPULSE(DYNE-SEC/CM2)
DISTANCE(KM)
PHASE SHIFT
50000000.00
24.00
.0000

FIG. 10.

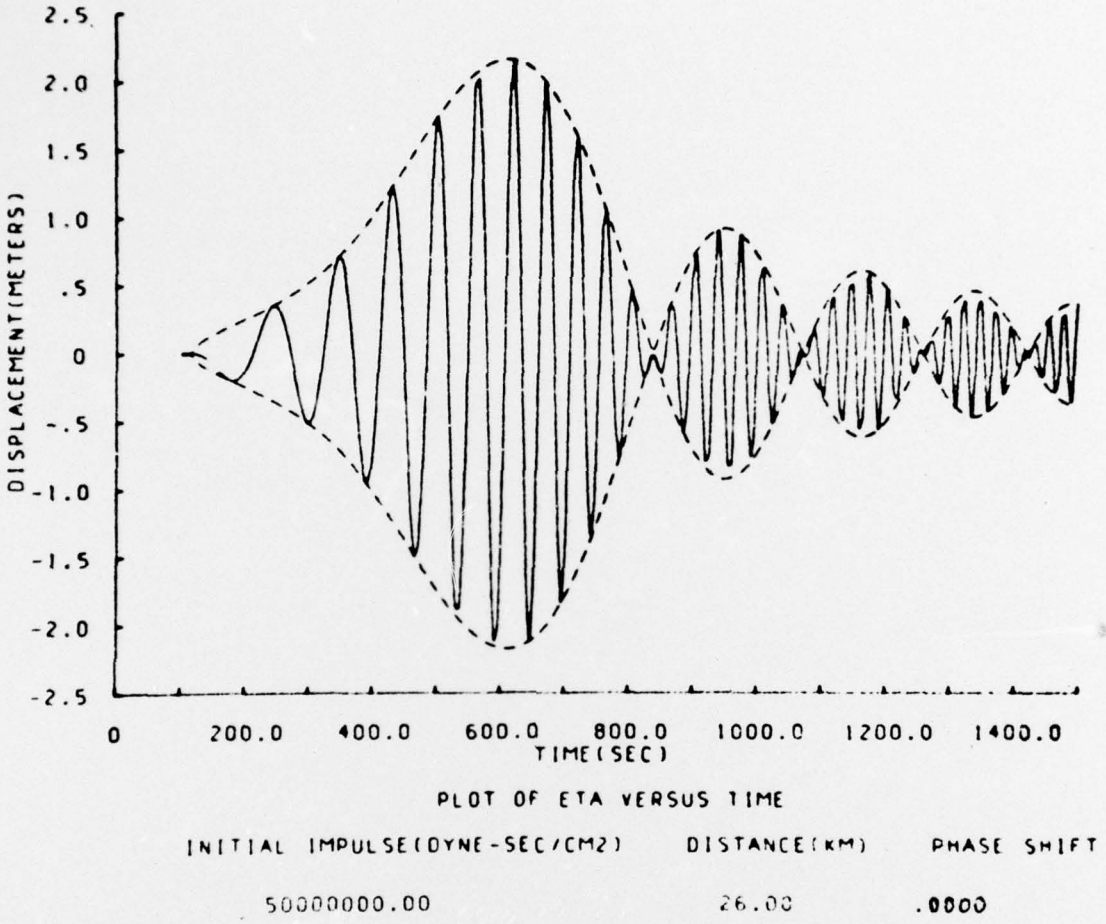
2.5
2.0
1.5
1.0
.5
0
-.5
-1.0
-1.5
-2.0
-2.5
DISPLACEMENT(METERS)
0
200.0
400.0
600.0
800.0
1000.0
1200.0
1400.0
TIME(SEC)
PLOT OF ETA VERSUS TIME
INITIAL IMPULSE(DYNE-SEC/CM2)
DISTANCE(KM)
PHASE SHIFT
50000000.00
26.00
.0000

FIG. 11.

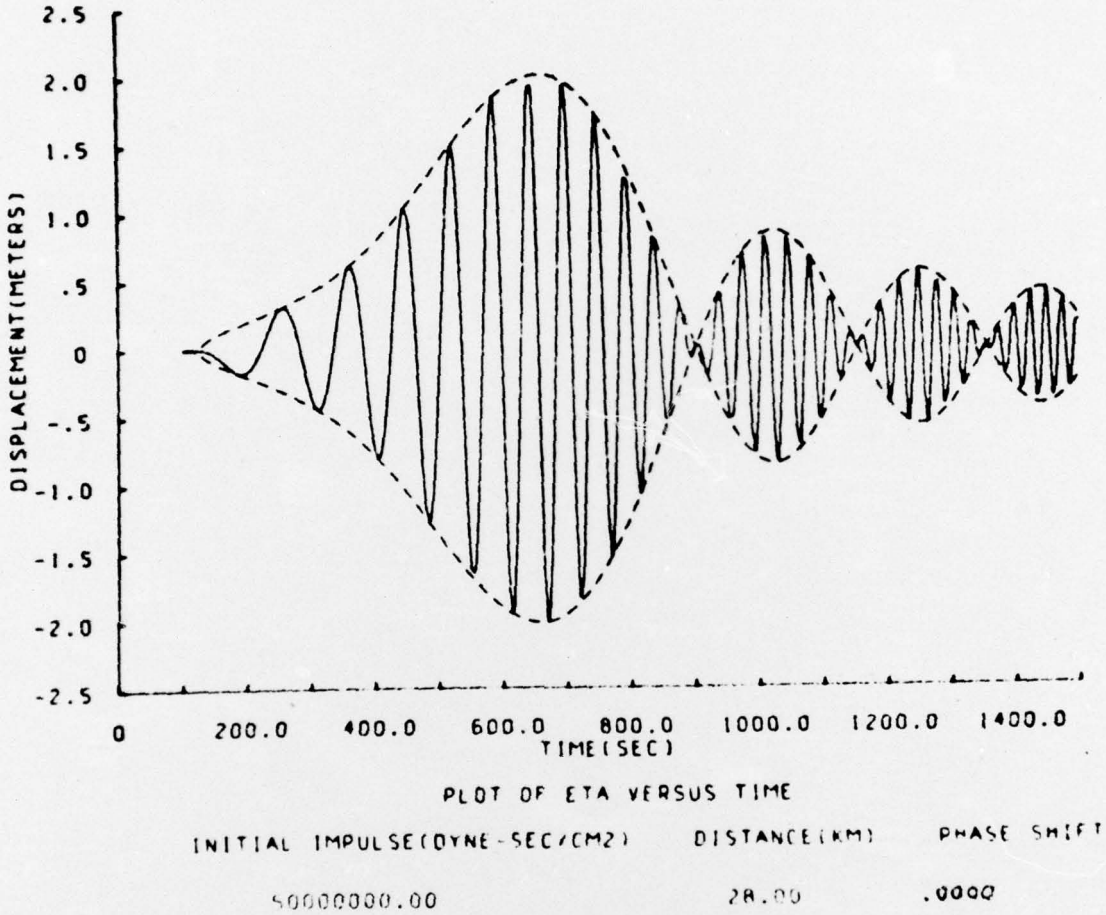
2.5
2.0
1.5
1.0
.5
0
-.5
-1.0
-1.5
-2.0
-2.5
DISPLACEMENT(METERS)
0
200.0
400.0
600.0
800.0
1000.0
1200.0
1400.0
TIME(SEC)
PLOT OF ETA VERSUS TIME
INITIAL IMPULSE(DYNE-SEC/CM2)
DISTANCE(KM)
PHASE SHIFT
50000000.00
28.00
.0000

FIG. 12.

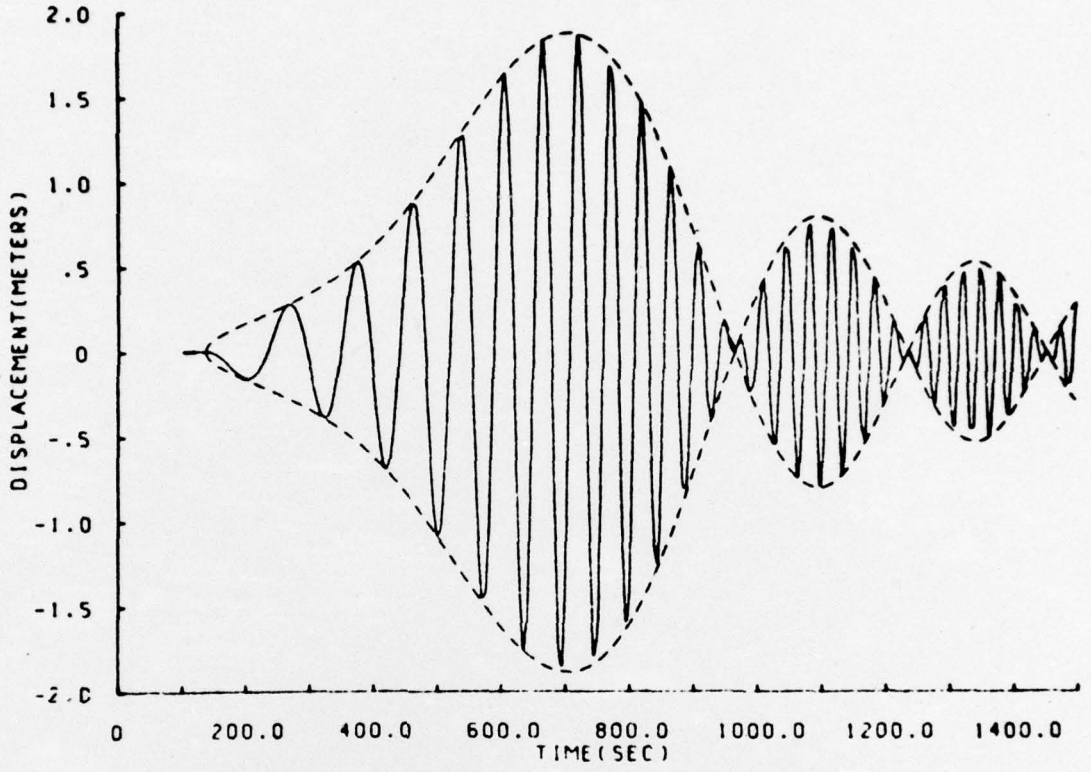

PLOT OF ETA VERSUS TIME

INITIAL IMPULSE(DYNE-SEC/CM2)	DISTANCE(KM)	PHASE SHIF
50000000.00	30.00	.0000

FIG. 13.

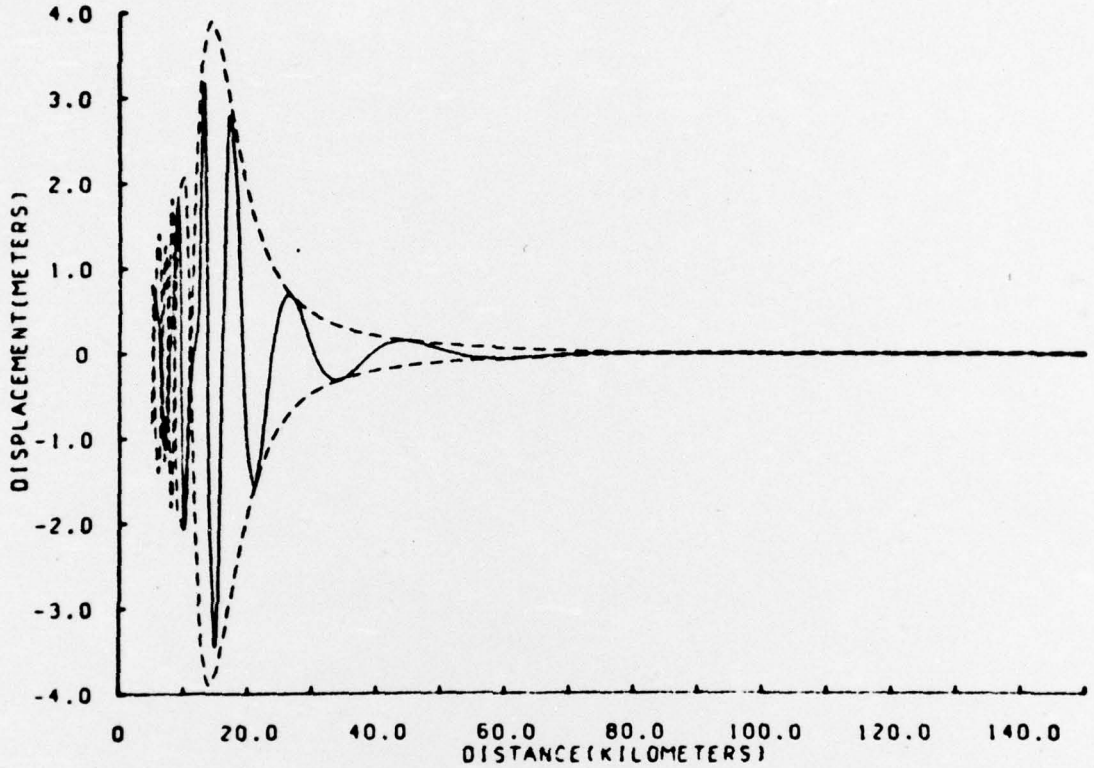

PLOT OF ETA VERSUS DISTANCE

INITIAL IMPULSE(DYNE-SEC/CM2)	TIME(SEC)	PHASE SHIFT
50000000.00	350.00	.0000

FIG. 14.

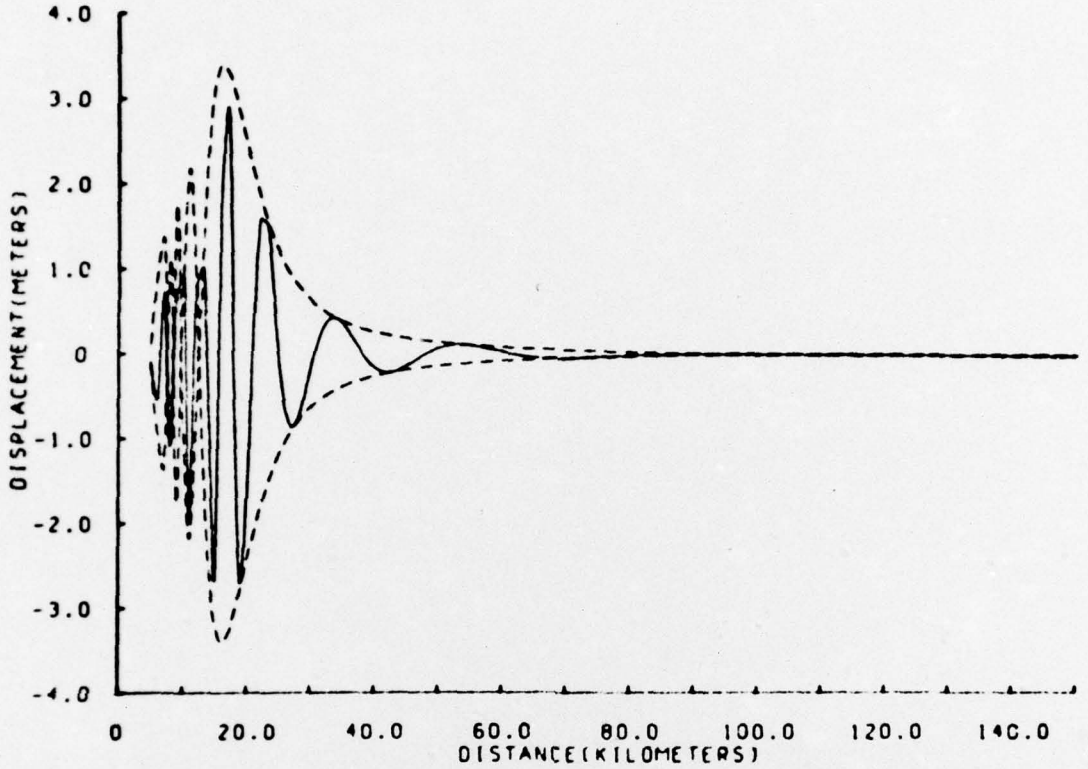
4.0
3.0
2.0
1.0
0
-1.0
-2.0
-3.0
-4.0
DISPLACEMENT(METERS)
0
20.0
40.0
60.0
80.0
100.0
120.0
140.0
DISTANCE(KILOMETERS)
PLOT OF ETA VERSUS DISTANCE
INITIAL IMPULSE(DYNE-SEC/CM2)
TIME(SEC)
PHASE SHIFT
50000000.00
400.00
.0000

FIG. 15.

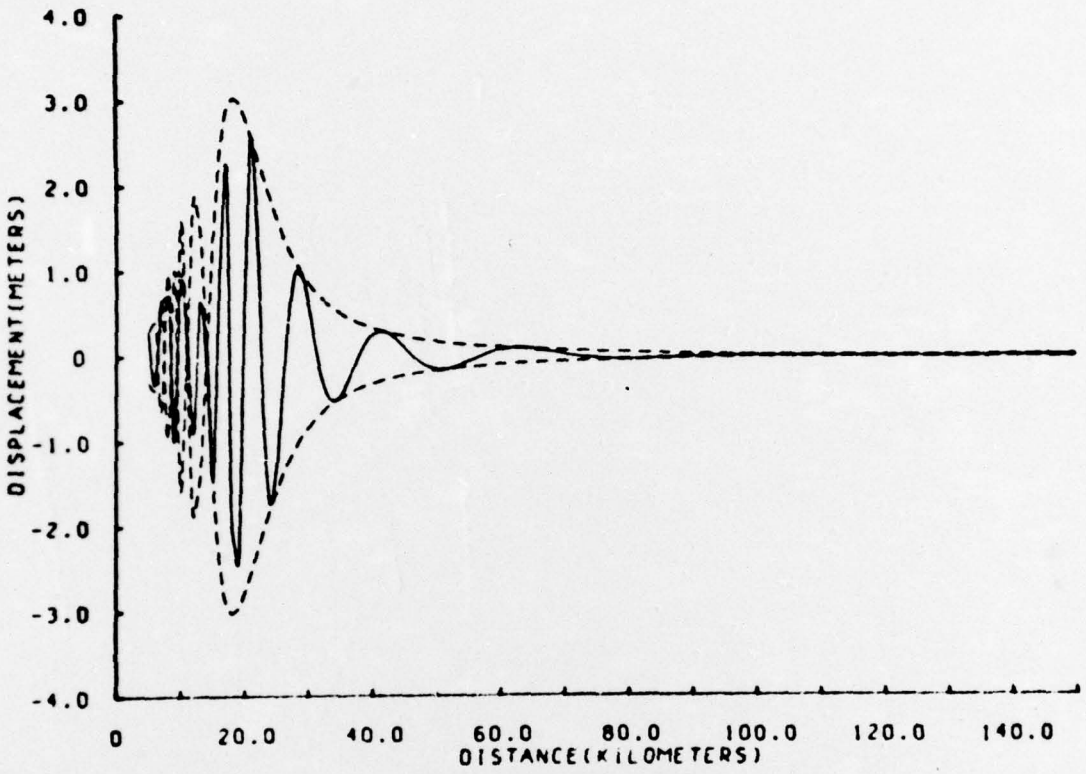

PLOT OF ETA VERSUS DISTANCE

INITIAL IMPULSE(DYNE-SEC/CM2)	TIME(SEC)	PHASE SHIFT
50000000.00	450.00	.0000

FIG. 16.

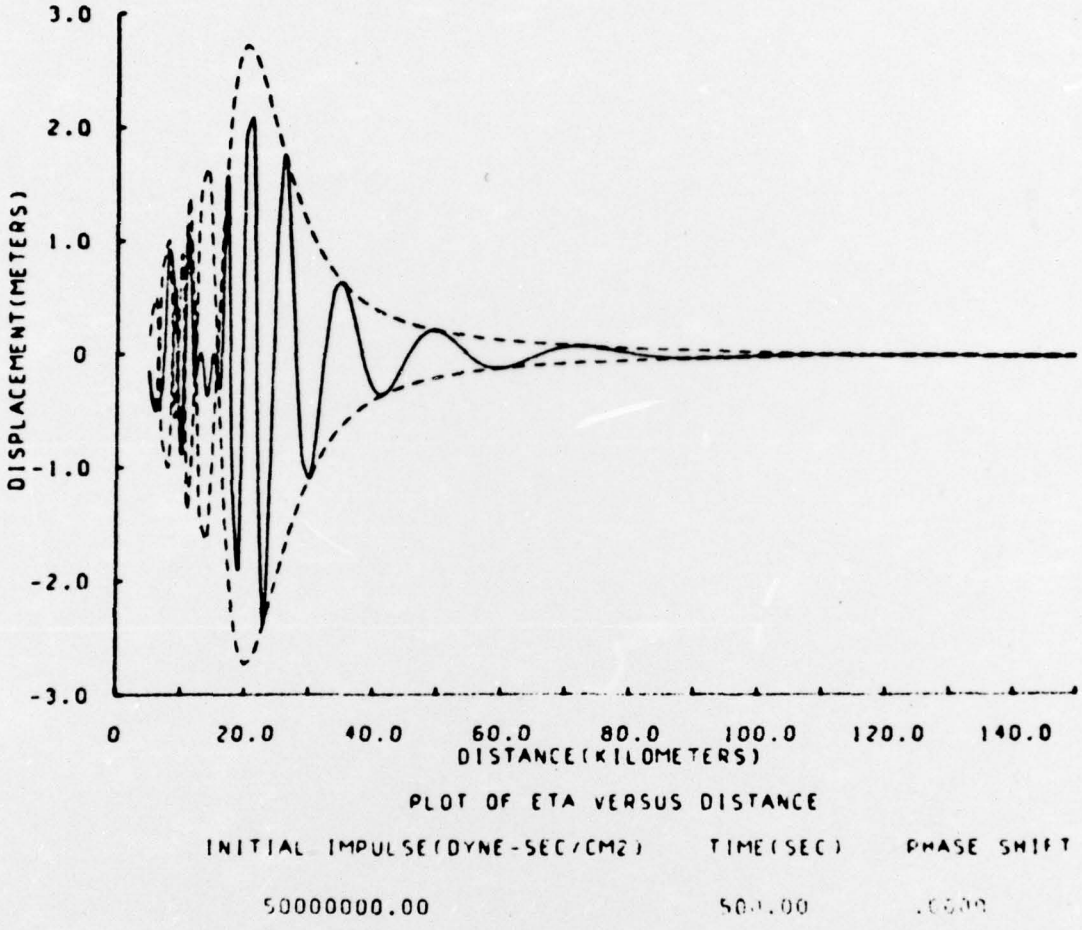
3.0
2.0
1.0
0
-1.0
-2.0
-3.0
DISPLACEMENT(METERS)
0
20.0
40.0
60.0
80.0
100.0
120.0
140.0
DISTANCE(KILOMETERS)
PLOT OF ETA VERSUS DISTANCE
INITIAL IMPULSE(DYNE-SEC/CM2)
TIME(SEC)
PHASE SHIFT
50000000.00
50.00

FIG. 17.

The figure below is the wave envelope and waves generated by an explosion of TNT on the ocean's surface. It was calculated using Kranzer and Keller's Theory, but is to be compared to an actual test run on Mono Lake in 1965. The radius of the charge was 34 inches (weighing approximately 5 tons), and the depth of the water was 130 feet (.04537 kilometers). Equation B.47 of Kriebel was used to calculate the effective radius of the explosion and the initial impulse impared to the water. Equation B.47 is:

$$R = (2)^{1/3} \times .17 \times \alpha = (2)^{1/3} \times 11 \times R_o$$

where $\alpha = 64.5 \times R_o$ for TNT; R_o is the charge radius; R is the effective radius

$$I_o = \frac{(2)^{1/3} \alpha p_a}{c_a}$$

where p_a is atmospheric pressure; c_a is the speed of sound in air; $\alpha = 64.5 \times R_o$ for TNT, and I_o imparted to the water is ten times I_o imparted to the waves.

In the actual test, $\eta_{max}(r) = 1800$ ft^2, so at 200 feet, $\eta_{max} = 2.74$ meters. Kranzer and Keller's result is fairly close to this result, with most of the error probably coming into the results through the approximation for the initial impulse.

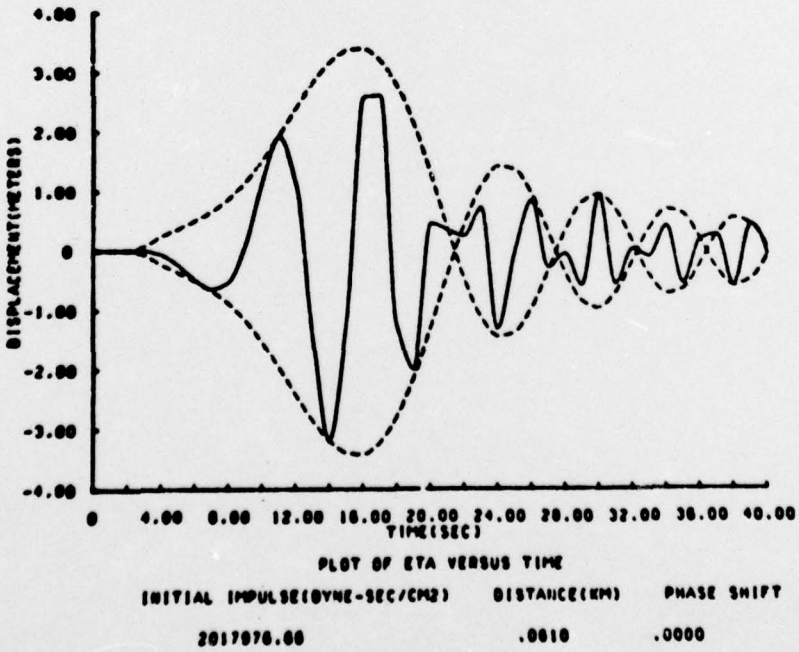

FIG. 18.

Comparison of theoretical and experimental data is shown below. The upper graph is the wave envelope measured 200 ft. away from a 125 pound charge in 1963 (Pinkston 1966). It is taken from Kriebel, Fig. A-2. The lower graph is generated using Kranzer and Keller's theory, with the initial impulse calculated using Eq. B.47 of Kriebel. (Note that Eq. B.47 gives the impulse imparted to the waves, but the impulse imparted to the water is ten times this amount.)

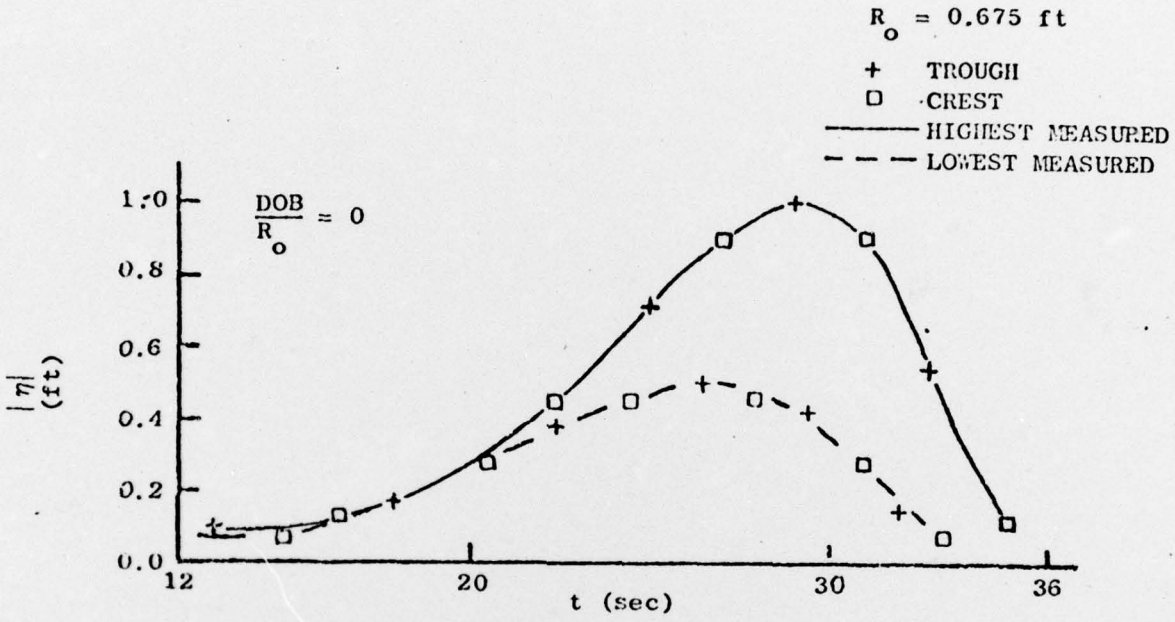

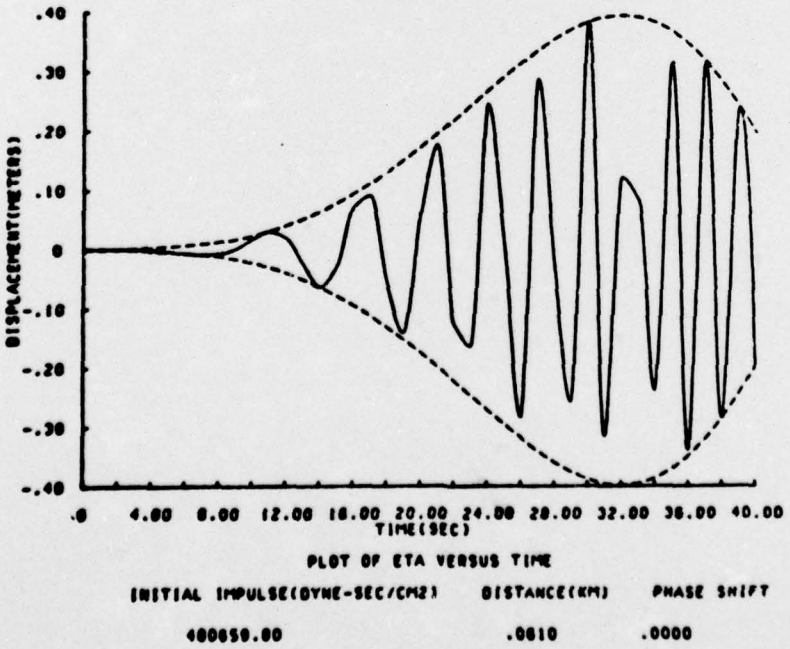

FIG. 19.